SARS-CoV-2 infected cells trigger an acute antiviral response mediated by Plasmacytoid dendritic cells in mild but not severe COVID-19 patients

Manon Venet[1*], Margarida Sa Ribeiro[1*], Elodie Décembre[1*], Alicia Bellomo[1*], Garima Joshi[1], Marine Villard[1], David Cluet[2], Magali Perret[1], Rémi Pescamona[1], Helena Paidassi[1], Thierry Walzer[1], Omran Allatif[1], Alexandre Belot[1], Sophie Assant[1], Emiliano Ricci[2], and Marlène Dreux[1$]

[1] CIRI, Inserm, U1111, Université Claude Bernard Lyon 1, CNRS, UMR5308, École Normale Supérieure de Lyon, Univ Lyon, F-69007, LYON, France

[2] Laboratory of Biology and Modeling of the Cell, Université de Lyon, ENS de Lyon, Université Claude Bernard, CNRS UMR 5239, Inserm U1293, Lyon, France.

[$] Corresponding author/lead contact; email: marlene.dreux@ens-lyon.fr, Tel.: + +33 426 23 38 34.

[*] Egal contributions as first co-authors.

6 Figures; 4 Supplementary Figures; **1 Table, 3 supplementary Tables**

Running title: pDC-mediated control of SARS-CoV2-infected cells is impaired in COVID-19 patients.

Keywords: Virus; SARS-Cov-2; Plasmacytoid Dendritic Cells; Interferon; TLR7; Cell contact/synapse.

Highlights

- pDCs are immune cells against SARS-CoV-2-infected cells
- pDC-mediated IFN-I/λ response against SARS-CoV-2 infected cells control COVID-19 progression
- pDC response by SARS-CoV-2 is restricted to IRF7-prioritized signaling leading to antiviral control
- pDC antiviral response directed toward contacting SARS-CoV-2-infected cells

Abstract

Type I and III interferons (IFN-I/λ) are key antiviral mediators against SARS-CoV-2 infection. Here, we demonstrate that the plasmacytoid dendritic cells (pDCs) are predominant IFN-I/λ source by sensing SARS-CoV-2-infected cells. We show that sensing of viral RNA by pDCs requires sustained cell adhesion with infected cells. In turn, the pDCs restrict viral spread by a local IFN-I/λ response directed toward SARS-CoV-2-infected cells. This specialized function enables pDCs to efficiently turn-off viral replication, likely by a concentrated flux of antiviral effectors at the contact site with infected cells. Therefore, we propose that pDC activation is essential to locally control SARS-CoV-2-infection. By exploring the pDC response in patients, we further demonstrate that pDC responsiveness correlates with the severity of the disease and in particular that it is impaired in severe COVID-19 patients. Thus, the ability of pDCs to respond to SARS-CoV-2-infected cells could be a key to understand severe cases of COVID-19.

Introduction

The innate immune system acts as the first line of defense for the sensing of viral infection. This involves rapid recognition of pathogen-associated molecular patterns (PAMPs), including viral nucleic acids, by pattern recognition receptors (PRRs). This recognition results in an antiviral response characterized by the production of type I and III (λ) interferons (IFN) and other pro-inflammatory cytokines, along with the expression of IFN-stimulated genes (ISGs). Whilst type I and III/λ IFNs interact with distinct receptors, they both induce similar signaling pathways and effector factors, thus referred herein to as the IFN-I/λ response **(Kim and Shin, 2021; Lazear et al., 2019)**. This host response suppresses viral spread by blocking the viral life cycle at multiple levels, hereby promoting virus clearance. The IFN-I/λ response also mediates immunomodulatory effects in surrounding tissues and imparts the onset of the adaptive immune response **(Crouse et al., 2015; Makris et al., 2017)**.

Severe acute respiratory syndrome coronavirus-2 (SARS-CoV-2) emerged in December 2019 and is responsible for the still-ongoing coronavirus disease 2019 pandemic **(Chan et al., 2020)**. Although most SARS-CoV-2-infected individuals experience asymptomatic to mild disease, others develop respiratory distress syndrome that is lethal in the most severe cases. Importantly, the IFN-I/λ response is now thought to be a critical host response against SARS-CoV-2 infection and its pathogenesis **(Grajales-Reyes and Colonna, 2020; Hadjadj et al., 2020; Kim and Shin, 2021; Sa Ribero et al., 2020; Saichi et al., 2021; Trouillet-Assant et al., 2020)**. Recent studies have shown that SARS-CoV-2 can evade from this initial control by the IFN-I/λ response *via* manifold inhibitory mechanisms interfering with both the sensing and the signaling pathways within infected cells (reviewed in **(Kim and Shin, 2021; Min et al., 2021; Park and Iwasaki, 2020; Sa Ribero et al., 2020)**), and *e.g.*, illustrated in **(Kimura et al., 2021; Lei et al., 2020; Miorin et al., 2020; Saichi et al., 2021 ; Wang et al., 2021; Xia et al., 2020)**). This immune evasion might lead to an increased viral load, followed by widespread inflammations **(Sa Ribero et al., 2020)**. Individual immune responses against viral infection can thus be extremely heterogenous, ranging from robust and fast IFN-I/λ production to impaired and fatal defect in IFN-I/λ-mediated immunity, thereby highlighting the importance of IFN-I/λ for host defense against respiratory infections. Timing of the IFN-I/λ production also plays a crucial role in related Coronaviruses (*e.g.*, MERS-CoV and SARS-CoV-1) **(Channappanavar et al., 2016)**. Delayed IFN-I/λ signaling

associated to robust virus replication indeed promotes the accumulation of pathological monocyte-macrophages, resulting in lung immunopathology, vascular leakage and suboptimal T cell responses **(Channappanavar et al., 2016).** Early reports on SARS-CoV-2 also suggest an association between severe COVID-19 and low level of IFN-I/λ but overproduction of inflammatory cytokines **(Hadjadj et al., 2020; Lucas et al., 2020; Yao et al., 2021a)**. Accordingly, deficiency, neutralization by anti-IFNα-receptor autoantibodies or viral-mediated inhibition of the IFN-I/λ response aggravates SARS-CoV-2 pathogenesis **(Asano et al., 2021; Bastard et al., 2021a; Bastard et al., 2021b; Bastard et al., 2020; King and Sprent, 2021; Lopez et al., 2021; Zhang et al., 2020)**. It is therefore critical to understand the regulation of the optimal production and activity of IFN-I/λ.

The plasmacytoid dendritic cells (pDCs) are a unique immune cell type specialized for rapid and massive production of IFN-I (approx. 1000-fold more than other cell types) and IFNλ **(Reizis, 2019)**. pDCs possess multiple adaptations to efficiently produce IFN-I/λ **(Blasius et al., 2010; Esashi et al., 2012; Reizis, 2019; Sasai et al., 2010; Webster et al., 2016)**. As pDCs are refractory to most viral infections, their response is not directly repressed by viral proteins. Thus, this aspect also contributes to the exceptional magnitude of pDC IFN-I/λ production **(Decembre et al., 2014; Reizis, 2019)**. The main viral-sensors responsible for pDC activation are Toll-like receptors (TLR)-7 and -9 that recognize viral RNA and DNA, respectively **(Reizis, 2019)**. A recent report suggested that pDCs activated by SARS-CoV-2 differentiate into cytokine- and IFN-secreting effector cells, in a TLR-dependent manner **(Onodi et al., 2021)**. Studies on related coronaviruses have demonstrated that pDCs migration into the lungs, and their rapid production of IFN-I is essential for the control of CoV lethal infections **(Cervantes-Barragan et al., 2007; Chen et al., 2010; Lucas et al., 2020)**. Nonetheless, how pDCs respond to SARS-CoV-2-infected cells and how this response evolves in the course of viral infection are still open questions.

Here, we explored the cellular mechanisms underlying the IFN-I/λ response against SARS-CoV-2 infection. Our results uncovered that pDCs establish cell contact with SARS-CoV-2 infected cells via $\alpha_L\beta_2$integrin/ICAM-1 adhesion complex and regulators of actin network. This physical contact between pDCs and infected cells is required for the pDC-mediated antiviral response via TLR7 recognition. Capitalizing on the identification of modalities of this previously-unsuspected activation mechanism, we further studied how pDC IFN-I/λ response associates with COVID-19 severity. We demonstrated that the differentiation of

pDC into different subsets with distinct phenotypes and functions is restricted when activated by contact with SARS-CoV-2-infected cells. Consistently, this pDC activation preferentially induces a local IFNI/λ response, leading to efficient antiviral control directed towards the infected cells.

Results

Robust activation of pDCs in response to SARS-CoV-2-infected cells.

Respiratory epithelial cells represent the first infected tissue in the course of SARS-CoV-2 infection. To investigate which hematopoietic cell type is primarily responsible for the IFN-I/λ response against SARS-CoV-2 infection, human peripheral blood mononuclear cells (PBMCs) isolated from healthy donors were cocultured with SARS-CoV-2-infected human lung-derived cells or exposed to their supernatants (SN). Human alveolar basal epithelial cell lines (Calu-3 cells and A549 cells expressing the angiotensin-converting enzyme 2, A549-ACE2 cells) were infected for 48 hours prior to the collection of their SN or cells for incubation or coculture with PBMCs (including pDCs), both for 16-18 hours. We found that PBMCs respond by a robust secretion of IFNα when cocultured with SARS-CoV-2-infected cells (**Figure 1A-B**). In contrast, the SN of SARS-CoV-2-infected cells failed to trigger IFNα secretion by PBMCs (**Figure 1A-B**). As expected from previous publications, SARS-CoV-2-infected cells did not produce themselves detectable level of IFNα **(Blanco-Melo et al., 2020; Li et al., 2021; Lucas et al., 2020; Vanderheiden et al., 2020; Yamada et al., 2021; Yao et al., 2021b; Zhou et al., 2020)**. Plasmacytoid dendritic cells (pDCs) are known to robustly produce IFN-I/λ, notably IFNα **(Reizis, 2019)**. In line with this, antibody mediated-depletion of pDCs from PBMCs abolished IFNα secretion in response to co-cultured SARS-CoV-2-infected cells (**Figure 1A-B;** line PBMC+/pDC-). To further demonstrate that pDCs are the major source of IFNα upon incubation with SARS-CoV-2-infected cells, pDCs were immuno-isolated from PBMCs (over 92% purity as we have previously reported **(Assil et al., 2019; Decembre et al., 2014)**). Purified pDCs potently produced IFNα in response to co-culture with SARS-CoV-2-infected cells, but not in the presence of uninfected cells (**Figure 1A-B)**.

Consistent with these results, we further showed that IFNα producer cells were markedly enriched in the cell population gated as pDC as compared to other hematopoietic cell types (non-pDCs) **(Figure 1C and S1A)**. Furthermore, IFNα expression level per pDC was very elevated (*i.e.,* 2-log increased of mean fluorescence intensity over background; sub-selected as IFNα^{hi}) (**Figure 1C, right panel)**. Most IFNα–positive pDCs concomitantly produced IFNλ in response to SARS-CoV-2-infected cells (**Figure 1C)**. Of note, the IFNα response mounted by pDCs in response to SARS-CoV-2-infected cells largely exceeded the one elicited by stimulation with TLR agonists *i.e.,* imidazoquinoline compound [R848] and

synthetic analog of double-stranded RNA polyinosinic-polycytidylic acid [polyI:C] (**Figure 1C)**.

In contrast, this synthetic agonist led to a more potent upregulation of surface expression of activation markers including the programmed cell death ligand-1 (PD-L1) and CD83 as compared to coculture with SARS-CoV-2-infected cells (**Figure 1D)**. This suggested that the pDC response to SARS-CoV-2-infected cells is likely qualitatively distinct from stimulation by soluble agonists, likely because PD-L1 and CD83 are both NF-κB-induced activation markers, and thus involving signaling distinct from the IFN-I/λ response **(Antonangeli et al., 2020; Berchtold et al., 2002)**. Next, we tested whether the sensing of SARS-CoV-2-infected cells required a productive infection of pDCs, using a recombinant SARS-CoV-2 infectious clone expressing mNeongreen reporter (icSARS-CoV-2-mNG **(Xie et al., 2020)**). No infection of pDCs (defined as CTV^+-pDCs; **Figure S1I)** was detected when in contact with icSARS-CoV-2-mNG-infected A549-ACE2 cells (**Figure S1I).** However, in the same coculture set up, infection by icSARS-CoV-2-mNG was readily detected in initially uninfected/naive RFP^+ A549-ACE2 cells, hence proving validation of the efficient viral transmission (**Figure S1I)**. The absence of productive infection of pDCs is consistent with previous observations made with different viruses and might be explained by the specialized function of pDCs for rapid and potent antiviral response leading to abortive infection **(Decembre et al., 2014; Onodi et al., 2021; Reizis, 2019; Webster et al., 2018)**.

Taken together, these results strongly suggest that IFNα is robustly produced only by pDCs *via* sensing of SARS-CoV-2-infected cells and that this sensing most likely induces a specific activation state in pDCs.

Short range sensing of infected cells via cell contact triggers the pDC IFNα response.

We observed that cell-free SN from SARS-CoV-2-infected cell types failed to trigger IFNα production by PBMCs (**Figure 1A-B**) or by purified pDCs **(Figure 1E-H**), even when used at a multiplicity of infection (MOI) of 5 per pDC. Furthermore, SARS-CoV-2 does not productively infect pDCs (**Figure S1I**). Distinct from a previous report and to avoid possible misinterpretation due to contamination by cell debris and/or floating cells **(Onodi et al., 2021)**, we selected MOI and incubation time for SARS-CoV-2 infection so that no cytolytic effect was detectable in infected human lung-derived cells when cells and SNs were collected for coculture with pDCs (see *Experimental procedures section*). To further determine if cell-to-cell contacts were required for the transmission of the immunostimulatory signal to pDCs,

we used transwell chambers containing SARS-CoV-2-infected cells and pDCs separated by a 0.4μm permeable membrane. This physical cell separation fully prevented IFNα production by pDCs (**Figure 1E-H**). Similar results were obtained for pDC stimulated by SARS-CoV-2-infected lung-derived cell lines Calu-3, A549-ACE2, H358-ACE2 as well as Huh7.5.1 cells, confirming that this feature was not cell type restricted (**Figure 1E-F and S1D-E**). Again, consistently with results shown in **Figure 1A-B** and previous reports **(Blanco-Melo et al., 2020; Li et al., 2021; Lucas et al., 2020; Vanderheiden et al., 2020; Yamada et al., 2021; Yao et al., 2021b; Zhou et al., 2020)**, none of the SARS-CoV-2-infected cell types released themselves detectable levels of IFNα (**Figure 1E-F**).

To further define the mechanisms underlying pDC activation upon contact with SARS-CoV-2-infected cells, we assessed the implication of cell adhesion complexes in this process. We focused on αL integrin and its ligand Intercellular Adhesion Molecule (ICAM)-1 (also called CD54) **(Rothlein et al., 1986)**, respectively highly expressed by pDCs and by various cell types, guided by previous studies on the regulation of pDCs in other infection contexts **(Assil et al., 2019)**. Antibody-mediated blockade of both α_L integrin and ICAM-1 greatly prevented pDC IFNα production (**Figure 1G**). The engagement of integrins by their ligands is known to induce local recruitment of the actin network. Notably Arp2/3 complex mediates actin nucleation by recruiting and branching actin filaments within network **(DeMali et al., 2002; DeMali et al., 2014; Rotty et al., 2013; Vicente-Manzanares et al., 2009)**. Pharmacological inhibition of Arp2/3 complex impaired IFNα production by pDCs in coculture with SARS-CoV-2-infected cells, in a dose dependent-manner (**Figure S1G)**. This suggested that cell adhesion-induced actin recruitment is likely involved in the structuration of cell contacts. Using specific TLR7 antagonist (*i.e.*, IRS661), we showed that the endosome-localized TLR7 sensor mediates the sensing of SARS-CoV-2-infected cells by pDCs (**Figure S1H**). Remarkably, similar levels of IFNα secretion were reproducibly obtained for pDCs isolated from the blood of a cohort of healthy donors (**Figure 1H**; distinct healthy donors as n=11 and n=15 for A549-ACE2 and Calu-3 cells respectively).

Together our results demonstrated that physical contacts between pDCs and SARS-CoV-2-infected cells are required for pDC IFNα production. This contact presumably involves cell adhesion mediated by $\alpha_L$integrin/ICAM-1 complexes and the actin network, and leads to a robust TLR7-dependent IFNα response by the pDCs.

The IFN-I/λ signature observed in patients at early time point of SARS-CoV-2 infection is associated with viral clearance.

Based on the importance of pDCs as the main cell type producing IFNα in response to SARS-CoV-2-infected cells, we sought to explore how this herein-uncovered mechanism for potent IFN-I/λ response is modulated in the course of the infection in patients and how it could relate to COVID-19 severity. A longitudinal study of IFN-I/λ response was done with different subsets of patients: *i)* critically ill, herein referred to as *Severe* patients, who presented acute respiratory distress syndrome or severe pneumonia at hospital admission and required mechanical ventilation in intensive care units, and *ii)* patients with mild symptoms (*i.e.,* low-grade fever, cough, malaise, rhinorrhea, sore throat), that group was sub-divided according to the days of sample collection post-symptom onset, *i.e., Mild early* for the first two weeks and *Mild late* at the later time points. Of note, most patients were SARS-CoV-2 positive in nasal swab samples by qPCR at sampling time in the *Mild early* group but not anymore or presenting low viral levels in the *Mild late* group. All patients and the analyzed time-points are listed in **Table 1** and **S1,** which provides information on the clinic and viral loads in nasal swab samples.

We quantified the IFN-I/λ levels in blood samples of infected patients at the transcriptional level (IFN-I signature by by Nanostring technology) and at the protein level for secreted IFNα, IFNλ1, IFNγ together with IL-6. Both approaches revealed an elevated IFN-I/λ response at early time points (within the first 10-11 days post-onset of symptoms) for all patients with mild symptoms, that seemed to vanish over time, mirroring the controlled decrease of the viral load (**Figure S2A** and **Table S1**). Of note, the level of the pro-inflammatory cytokine IL6 was elevated in *Severe* patients (**Figure S2A** and **Table S1**), in line with the previously reported production of pro-inflammatory cytokines in COVID-19 patients **(McGonagle et al., 2020; Vanderbeke et al., 2021).**

Overall, the patients experiencing mild infection demonstrated high IFN-I/λ blood levels at early time-points. Furthermore, the inflammatory response appeared to be correlated with disease severity, in agreement with previous reports **(Galani et al., 2021; Hadjadj et al., 2020; McGonagle et al., 2020; Vanderbeke et al., 2021)**.

The responsiveness of pDCs to SARS-CoV-2-infected cells is impaired in infected patients.

We then determined the ability of PBMCs isolated from the different groups of patients to

respond to *ex vivo* stimulation by SARS-CoV-2-infected cells. As our results pointed out the importance of pDCs in the IFN-I/λ response mounted against SARS-CoV-2 infected cells, we primarily analyzed pDCs as well as other cell types selected for their potential to play pivotal first defense against viruses. Especially, the Th1-promoting myeloid/conventional dendritic cell subset (mDC1), which produces IFNλ *via* TLR3-mediated recognition of viral RNA **(Lauterbach et al., 2010; Yoshio et al., 2013)** and the Th2-promoting myeloid/conventional DC subset (mDC2) and monocytes *i.e.*, Human Leukocyte Antigen – DR isotype (HLA-DR)$^{+}$CD14^{+}populations known to produce proinflammatory cytokines **(Bosteels et al., 2020; Leal Rojas et al., 2017; Merad et al., 2013; Mildner and Jung, 2014; Wong et al., 2011)**. This response was compared to the one induced by agonists. Agonists were selected in accordance with the targeted cell types: TLR7/TLR3 agonist [polyI:C/R848] for pDC (TLR7) and the mDC1 (TLR3), and TLR-4 agonist [lipopolysaccharide; LPS] for mDC2 and HLA-DR^{+}CD14^{+} populations. A group of *healthy* donors comprising similarly treated samples was used as reference. Post-stimulation, we performed a multiparametric flow cytometry analysis to define the profiles of cell surface expression of several activation markers along with intracellular cytokines. These responses were assigned to different pivotal innate immune cells by designing a combined panel of cell type markers, along with the exclusion of other cell types (see gating strategy in **Figure S2B)**.

Principal component analysis (PCA) of the flow cytometry datasets was performed within each cell population and stimulation condition to test whether differences in activation and cytokine expression could be linked to disease severity (**Figure 2**). PCA allows to reduce high dimensional data into principal components that maximize the variance of the projected data and potentially identify the underlying factors associated with it. In the upper panels (**Figure 2**), each patient is placed with respect to its distribution in the first two principal components (PCs), which explain most of the data variance. In the lower panels, vectors corresponding to the eigen decomposition of the data covariance matrix are depicted to identify features that explain the observed variance. For pDCs analyzed in the unstimulated condition, the first two principal components (PCs) revealed a differential segregation of the patients: the *Severe* group (in red), and to some extent *mild early* group (in purple) were mainly spread across the first PC (which was explained by IFNα, CD80 and PD-L1), while *healthy* and *Mild late* individuals were tightly clustered in both PCs (**Figure 2A**, left panels). An opposite segregation of the patient groups was observed in pDCs when PBMCs were cocultured with SARS-CoV-2-infected cells. Especially, this stimulation induced a spread

across the first PC (mainly driven by IFNα/IFNα^{hi} and CD83 expression) of patients from the *Mild* and *healthy* groups, in accordance with the pDC ability to respond to SARS-CoV-2-infected cells (**Figure 2A**, middle panels). Of note, the *healthy* individuals were spread across the two PCs, whereas the *Mild early and Mild late* groups dispersed primarily along the first PCs. On the contrary, individuals from the *Severe* group were spread across the second PC (driven by CD80 and PD-L1 expression). Regarding pDC response to synthetic agonist, all groups were similarly spread across the first two PCs, while the *Severe* group was tightly grouped within the second PC (driven by IFNλ expression) (**Figure 2A**, right panels). These results suggested that pDCs from *Severe* individuals display differences in activation markers and cytokine expression compared to individuals from all the other groups, especially when stimulated by SARS-CoV-2-infected cells. PCA analysis performed on mDC1 subset demonstrated less marked contrast among the patient groups upon stimulation by SARS-CoV-2-infected cells, although the *Severe* group appeared more tightly grouped across both PCs (**Figure 2B;** middle panels). Upon agonist stimulation, mDC1 from the *Severe* group were also tightly grouped within the second PC (driven by IFNλ1, CD83 and PD-L1; **Figure 2B;** right panels). PCA analyses of mDC2 and HLA-DR^{+}CD14^{+} populations revealed no marked contrast across the patient groups in the unstimulated condition and SARS-CoV-2 stimulation, while the *Severe* individuals tended again to be grouped in agonist stimulation (**Figure 2C-D**).

Taken together, our results highlighted that the contrast between *Severe* patients and the other groups is more pronounced in pDCs than in other PBMC subsets and upon stimulation by SARS-CoV-2-infected cells.

COVID-19 severity primarily associated with a blunted pDC IFNα response to SARS-CoV-2-infected cells.

We further analyzed the expression of activation markers and cytokines individually at the single-cell level in the defined cell types, focusing first on markers identified as driving forces in the PCA analyses. In keeping with results of **Figure 1**, the frequency of IFNα^{+} pDCs greatly increased in response to SARS-CoV-2-infected cells in the *healthy* donor group (**Figure 3A,** green arrow). In sharp contrast, pDCs from *Severe* patients failed to be activated by SARS-CoV-2-infected cells as similarly revealed by the detection of IFNα^{+}, IFNλ^{+} and CD83^{+} pDC (**Figure 3A-C**; red bars and arrows). Of note, a strong basal level of pDC IFNα expression was observed in the absence of stimulation for the *Severe* patients. The response to agonist stimulation was also greatly diminished in pDCs from *Severe* patients compared to

healthy donors and patients with *mild* symptoms, as shown by the level of activation markers (CD83, CD80 and PD-L1; **Figure 3C-E**; red arrows).

In line with the results obtained with pDCs, expression of IFNλ1 was barely detectable in the mDC1 subset of *Severe* patients upon stimulation by SARS-CoV-2-infected cells and agonists, comparatively to the other groups (**Figure 3F;** red arrows). Further, our data showed a potent upregulation of IL6 by HLA-DR$^+$CD14$^+$ subset upon agonist treatment in *Severe* patients and *Mild early* (**Figure 3G**). HLA-DR$^+$CD14$^+$ population represents a highly frequent cell subset of non-mDC2 (*e.g.*, among the gated live cells$^+$ lin$^-$ HLA-DR$^+$*:* 65.7% are HLA-DR$^+$CD14$^+$ population and the exclusion of mDC2 represent only 4.85%; **Figure S2A)**. In accordance, a high frequency of IL6$^+$ cells was also observed for the non-mDC2 populations (**Figure 3G**, right panel). Likewise, *Severe* patients presented an elevated level of blood IL6 (**Figure S2A**). These results are consistent with the previously reported production of pro-inflammatory cytokines by monocytic cells in patients with severe disease **(Hadjadj et al., 2020; Vanderbeke et al., 2021)**, and provided further insights into the differential responses of other cells.

We thus sought to define the dynamics of the response in COVID-19 patients. First, kinetic analyses in *Mild* patients revealed an elevated detection of pDC IFNα$^+$ levels in absence of stimulation that vanished over time while, relatively, their ability to respond to SARS-COV-2-infected cells increased at late time-points (**Figure 3H,** left panel). Basal level of pDC IFNα$^+$ (*i.e.,* in absence of stimulation) was also observed for *Severe* patients and associated to a limited induction in response to SARS-COV-2-infected cells at all analysed time-points (**Figure 3H,** right panel). Kinetic analysis was performed for a *Severe* patient, who had anti-IFNα antibody detected in the blood (patient description included in **Table 1**; legend) **(Asano et al., 2021; Bastard et al., 2021a; Bastard et al., 2021b; Bastard et al., 2020; King and Sprent, 2021; Lopez et al., 2021; Zhang et al., 2020)** . It showed that the ability of pDC to respond to stimulation was blunted in this patient (**Figure 3H,** right panel; represented by starts with yellow-center).

Together our results demonstrated that the monocytic subset likely contributes to an exacerbated pro-inflammatory response implying notably IL6 production, but that is presumably not triggered directly by the contact with SARS-CoV-2-infected cells. As opposed, impaired IFN-I/λ response following cell contact with pDCs from *Severe* patients, including those with anti-IFNα, suggested a '*silencing/exhaustion*' of pDCs in this context. This might be due to the lack of an amplification-loop by ISG resulting in lower activated

state and IFNα production by pDCs and to some extent, similarly, IFNλ1 expression by mDC1.

Limited pDC differentiation and cytotoxic activity induced by the contact with SARS-CoV-2-infected cells compared to stimulation by cell-free agonists

As we found that pDC activation is a salient feature that correlates with severe COVID-19, we aimed to determine how the contact with SARS-CoV-2-infected cells impacts the varied downstream signaling and function of pDCs. First, we analyzed the expression of pDC surface molecules enabling the stimulation of adaptive responses, namely HLA-DR, an MHC class II cell surface receptor driving the activation of $CD4^+$ T cells, and the B cell ligand CD70 expressed by pDCs and known to interact with CD27 and to induce proliferation and differentiation of B cells into plasmablast **(Shaw et al., 2010)**. Our results showed that pDCs upregulated both surface molecules in response to contact with SARS-CoV-2-infected cells, although at a lower level compared to stimulation by cell-free virus (influenza virus; flu) and synthetic agonists of TLR7/3 [R848/polyI:C; R/p] and TLR7 [imiquimod; IMQ] (**Figure 4A-B**). Similarly, surface expression of CD83, an activation marker for antigen presenting cells **(Gomez et al., 2004; Li et al., 2019)**, was induced upon contact with SARS-CoV-2-infected cell and jointly expressed with PD-L1 by the same pDC subset (**Figure 4C**). These results obtained with purified pDCs are in agreement with results obtained with pDCs present in PBMCs and cocultured with SARS-CoV-2-infected cells (**Figure 1D**). Of note, SN from SARS-CoV-2-infected cells induced HLA-DR, CD83 and PD-L1 expression, yet not as potently as other soluble agonists (**Figure 4A and 4C**).

pDCs are now recognized to be an heterogeneous population composed of subsets endowed with diversified functions **(Abbas et al., 2020; Alculumbre et al., 2018; Bryant et al., 2016; Matsui et al., 2009; Onodi et al., 2021; Reizis, 2019; Villani et al., 2017)**. As stimulation of pDCs can impact the frequency and phenotype of these subsets, we assessed the expression of a set of surface molecules previously assigned to define specific subpopulations of pDCs *i.e.*, CD2, CD5, AXL, CD80 and PD-L1 **(Alculumbre et al., 2018; Bryant et al., 2016; Matsui et al., 2009; Onodi et al., 2021; Reizis, 2019; Villani et al., 2017)**. $CD2^{hi}$ pDCs have a survival advantage and are able to efficiently trigger proliferation of naive allogenic T cells **(Bryant et al., 2016; Matsui et al., 2009; Zhang et al., 2017)**. Stimulation of pDCs by contact with SARS-CoV-2-infected cells did not impact the frequency of $CD2^{hi}$ pDCs, and this $CD2^{hi}$ subset displayed an activation profile similar to the one of $CD2^{low}$ subset (**Figure**

4D and S4B). $CD2^{hi}$ $CD5^{+}$ AXL^{+} pDCs were recently proposed as a defined subset that display limited IFN-I production capacity but can potently activate T cells **(Villani et al., 2017).** The $CD2^{hi}$ $CD5^{+}$ AXL^{+} pDCs, which represent a very scarce subpopulation of pDCs **(Villani et al., 2017)**, modestly decreased upon stimulation by SARS-CoV-2-infected cells, their SN or TLR-agonists, yet whether this intriguing decrease is relative to the activated state of pDCs requires further investigation (**Figure S4C**). We then addressed the diversification of pDCs into functionally distinct populations defined by PD-L1/CD80 expression. In agreement with previous reports, the stimulation by cell-free agonists and influenza virus triggered the differentiation into both PD-$L1^{+}CD80^{+}$ and PD-$L1^{-}CD80^{+}$ pDC subsets **(Alculumbre et al., 2018; Onodi et al., 2021)**. In sharp contrast, direct contact with SARS-CoV-2-infected cells restricted the differentiation of pDCs towards PD-$L1^{+}$ $CD80^{-}$ subset (**Figure 4E**).

Collectively, these results revealed that, unlike activation by cell-free viruses and agonists, direct activation of pDCs by SARS-CoV-2-infected cells restricted their differentiation into specific functional subsets.

We observed that pDCs expressed PD-L1 upon stimulation by SARS-CoV-2-infected cells. Therefore, we further examined the induction of cytotoxic/immune-suppressive activity of pDCs. In keeping with the previously-reported induction of membrane-bound TNF-related apoptosis-inducing ligand (mTRAIL) expression by pDCs upon viral stimulation (*e.g.,* HIV) **(Achard et al., 2017; Colisson et al., 2010; Gandini et al., 2013)**, we found that mTRAIL was readily co-expressed along with PD-L1 and CD83 upon stimulation by influenza virus and synthetic agonists. Nonetheless, mTRAIL upregulation was more limited upon pDC stimulation by SARS-CoV-2 compared to stimulation by cell free agonist (**Figure 4F,** total % of the bars). Moreover, the frequencies of Annexin V^{+}/7-ADD^{+} apoptotic Calu-3 and A549 cells in cocultures with pDCs were similar between infected (*i.e.,* pDC activation) and uninfected (*i.e.,* no pDC activation) conditions, hence suggesting that mTRAIL expression on activated pDCs did not endow these cells with cytotoxic activity. (**Figure 4G**). In line with this, the contact with activated pDCs did not markedly impact the viability of the cocultured SARS-CoV-2-infected cells (*i.e.,* when comparing condition with or without the anti-α_L integrin, which inhibits contact and pDC activation), nor the viability of activated pDCs themselves, even when analyzed after 48 hours of coculture (**Figure 4H**).

Overall, these results showed that activation of pDCs by SARS-CoV-2-infected cells did not induce cytotoxic/immune-suppressive activity, mostly leading to a restricted diversification into functional pDC subsets and likely toward to their ability to robustly produce IFN-I/λ.

pDC activation by SARS-CoV-2-infected cells primarily leads to the antiviral state *via* IFN-I/λ production.

We then sought to examine deeper the signaling pathways at play in pDCs upon activation by coculture with SARS-CoV-2-infected cells. TLR7-dependent activation of pDCs can induce a 'bifurcated' signaling leading to *(1)* IFN-I/λ production mostly *via* IRF7-related signaling and other cytokines and *(2)* activation molecules *via* NF-κB-pathway **(Reizis, 2019; Webster et al., 2018)**. We noticed that expression of the activation marker HLA-DR, CD70, CD83, mTRAIL by pDCs was weaker when induced by contact with SARS-CoV-2-infected cells compared to soluble agonist stimulation (**Figure 4**). These markers/proteins are primarily regulated by NF-κB-mediated signaling **(Table S3) (Antonangeli et al., 2020; Berchtold et al., 2002)**. To further define the signaling active in pDCs, we quantified transcripts levels of representative key effectors regulated by IRF/IFN-I signaling (*i.e., mxA, isg15* and *ifnλ) versus* those primarily regulated by NF-κB-pathway (*i.e., il-6* and *tnfα)* (**Table S3**) **(Liu et al., 2017; Mesev et al., 2019)**. Cocultures of pDCs and SARS-CoV-2-infected cells induced more the IRF7/IFN-I-regulated molecules than the representatives of the NF-κB-pathway (**Figure 5A**). This was again confirmed by the quantification of secreted cytokines in the cocultures, demonstrating higher levels of IRF7/IFN-I-regulated IFNλ1/2/3 compared to TNFα (**Figure 5B** compared to **5C**). This observation was also in agreement with the high level of secreted IFNα in similar experiments (**Figure 1E-H**). Of note, no detectable cytokine and low level of transcript upregulation were detected in SARS-CoV-2-infected cells in the absence of pDCs, or when pDCs were stimulated by SARS-CoV-2 SNs. In these assays, the low activation level of the NF-κB-pathway and/or its variability among different infected cell types can be explained by a contribution of the infected cells, as a feedback loop of the response to activated pDCs. Hence, we assessed cytokine expression at single-cell level by flow cytometry in the gated pDCs (**Figure S4A**). Stimulation by SARS-CoV-2-infected cells elicited higher frequency of IFNα^+ pDCs compared to TNFα^+ pDCs (**Figure 5D**). Remarkably, almost all TNFα^+ pDCs were also IFNα^+, possibly implying an activation of the NF-κB-pathway subsequent to IRF7/IFN-I response. Again, this result contrasted with the limited frequency of IFNα^+ pDCs in response to cell-free agonist (**Figure 5D**). Similar

analysis performed for IFNα^+ combined with IFN$\lambda1^+$ also revealed that virtually all IFN$\lambda1^+$ pDCs were IFNα^+ (**Figure 5E**).

Collectively, our data provided evidence that, in contrast to stimulation with cell-free viruses and agonists, the pDC response to contact with SARS-CoV-2-infected cells is biased towards IRF7-mediated signaling that leads to a robust IFN-I/λ production.

The pDC antiviral response is directed toward the contacting SARS-CoV-2 infected cells.

As the response to SARS-CoV-2-infected cell primarily induced IFN-I/λ antiviral signaling, we next aimed to define how the pDC response inhibits viral propagation. pDCs were cocultured for 48 hours with icSARS-CoV-2-mNG-infected A549-ACE2 cells (mNG$^+$) and uninfected A549-ACE2 RFP$^+$ cells, and viral spread was quantified by flow cytometry. The results demonstrated that the pDC response readily prevented viral spread from mNG$^+$ infected cells to initially uninfected RFP$^+$ cells, whilst also slightly diminishing the replication in mNG$^+$ infected cells during the coculture incubation time (**Figure 5F-G**). The inhibition of contact between pDCs and infected cells *via* blockage of α_L integrin restored viral propagation to levels comparable to those measured in the absence of pDC (**Figure 5F-G**). This indicated that the establishment of cell-contact *via* adhesion molecules is required for pDC-mediated antiviral response.

Interestingly, the impact of pDC antiviral response on cells infected prior to coculture was quite modest as compared to the spread to uninfected cells, likely owing to the inhibition of IFN-I/λ signaling by SARS-CoV-2 **(Chen et al., 2021; Yang et al., 2020)**. Therefore, we hypothesized that the reduction could be more potent if infected cells were directly in contact with pDCs as such contact could allow a concentrated antiviral response toward the infected cell. To test this hypothesis, we established an assay of 24 hour-long live-imaging of the coculture of pDCs (stained with CM-Dil; red) and icSARS-CoV-2-mNG infected cells (mNG$^+$; green) using spinning-disk confocal microscopy. As depicted by the example of time-sequence imaging (**Figure 6A**), pDC contact with mNG$^+$ infected cells lead to a control of viral replication in the targeted infected cells, reflected by the decreased mNG fluorescent reporter signal. We controlled that these infected cells, although not mNG$^+$ anymore, were still physically present by using enhanced fluorescent signal analysis (**Figure 6A**; lower panels). Viral control by pDCs was seen for pDC/infected cell contacts starting at different time points in the course of the coculture (*i.e.*, up to 14 hours after record onset). Similar analysis performed for several infected cells, either in contact with pDC *versus* not in contact,

revealed that the decrease in viral replication (*i.e.*, mNG fluorescence intensity) was observed only for infected cells directly in contact with pDCs (**Figure 6B, 6D-E**). Of note, live-tracking of mNG fluorescence intensity performed in infected cells cultured without pDCs, provided the basal level of the mNG fluorescence intensity (done simultaneously with record of coculture with infected cells). This basal level was comparable to the one measured in infected cells cocultured with pDCs that were not in direct contact with the latter (**Figure 6C-D**). pDCs established long-lasting contact with infected cells *i.e.*, mostly above 10 hours, and accordingly, the diminution of the mNG fluorescence intensity was detected several hours after the onset of contact, likely owing to the time-window needed to decrease viral replication (**Figure 6E-F**).

Overall, these results demonstrated that pDCs established sustained contact with SARS-CoV-2 infected cells *via* $\alpha_L\beta_2$integrin/ICAM-1 adhesion complex leading to an efficient antiviral response directed toward the infected cells that shut down viral replication.

Discussion

Here we demonstrate that pDCs are the key mediators of the IFN-I/λ response against SARS-CoV-2-infected cells. Moreover, our study exploring the responsiveness of PBMCs from COVID-19 patients establishes that pDC functions are of pivotal importance against COVID-19 severity. The sensing of SARS-CoV-2-infected cells by pDCs is mediated by the establishment of sustained contacts *via* cell adhesion molecules. These cell-cell contacts are required to enable the sensing of viral RNA by endolysosome-localized TLR7 and to restrict viral spread. This scanning function of pDCs does not involve their productive infection for immune surveillance of infected cells. We further demonstrate that pDC activation by contact with SARS-CoV-2-infected cells is characterized by IRF7/IFN-I/λ-prioritized signaling, while passively excluding NF-κB-mediated responses. The pDC-mediated IFN-I/λ response is targeted towards SARS-CoV-2 infected cells. This specialized function thus enables pDCs to efficiently turn-off viral replication, likely owing to a concentrated efflux of antiviral effectors at the contact site with infected cells.

pDCs critically control viral replication and the outcome of COVID-19 severity

Insights on several hallmarks of IFN-I/λ pathway as being critical in COVID-19 severity are emanating from recent publications. First, neutralizing autoantibodies against several cytokines and genetic defects affecting the IFN-I pathway have been identified in life-threatening COVID-19, as autosomal disorders of IFN-I immunity and autoantibodies underlie at least 10% of critical COVID-19 pneumonia cases **(Asano et al., 2021; Bastard et al., 2021a; Bastard et al., 2021b; Bastard et al., 2020; King and Sprent, 2021; Lopez et al., 2021; Zhang et al., 2020)**. Second, patients with severe diseases exhibit reduced circulating pDCs and low plasma IFN-I/λ levels when compared to mild COVID-19 patients **(Hadjadj et al., 2020; Lucas et al., 2020; Yao et al., 2021a)**. Third, IL-3, which increases innate immunity likely by promoting the recruitment of circulating pDCs into the airways, is reduced in the plasma of patients with high viral load and severity/mortality **(Benard et al., 2021)**. This evidence highlights that several biomarkers of IFN-I/λ response are diminished in COVID-19 patients, and hereby points to pDCs as a primary candidate in the progression of COVID-19. Here, using an original approach to study innate immunity in *ex vivo*-stimulated PBMCs from COVID19 patients, we report that the functionality of pDCs is markedly blunted in severe patients, as observed upon their stimulation by SARS-CoV-2-infected cells as well as other TLR agonists.

pDC effector functions against SARS-CoV-2.

pDCs comprise distinct subpopulations capable of varied functions and efficacy levels to mount an IFN-I/λ response **(Abbas et al., 2020; Alculumbre et al., 2018; Bryant et al., 2016; Matsui et al., 2009; Onodi et al., 2021; Reizis, 2019; Rhodes et al., 2019; Villani et al., 2017)**. Viral infections and attendant inflammation potentially impact the frequency and functionality of the distinct pDC subpopulation including effect on pDC renewal **(Abbas et al., 2020; Alculumbre et al., 2018; Macal et al., 2018)**. Such modulations could be imprinted either by the micro-environment *via* crosstalk with immune cells, or by pDC activation itself.

We now report that neither pDC subpopulation frequencies nor their distinct ability to respond to SARS-CoV-2 are impacted by stimulation and contact with SARS-CoV-2-infected cells. This is illustrated for $CD2^{low}$/$CD2^{hi}$ pDCs that display similar activation profile upon stimulation with SARS-CoV-2-infected cells, and the frequency of $CD2^{+}CD5^{+}AXL^{+}$pDC-like, although their low number limit this analysis.

Interestingly, when comparing stimulations by contact with SARS-CoV-2-infected cells *versus* cell-free activators (*i.e.,* viruses and synthetic agonists), we found that the differentiation of pDCs defined by CD80 and/or PD-L1 expression are readily distinguishable depending on the TLR7 inducers. Whilst pDCs diversify towards all the different PD-L1/CD80 subsets upon cell-free stimulation (agonist and virus) in agreement with prior publications **(Alculumbre et al., 2018; Onodi et al., 2021)**, the contact with infected cells restricts their evolution to PD-$L1^{+}CD80^{-}$ subsets. Of note, previous reports suggested that PD-$L1^{+}CD80^{-}$ pDCs are more efficient for IFN-I response compared to the other subsets **(Abbas et al., 2020; Alculumbre et al., 2018; Onodi et al., 2021)**.

In accordance with this phenotype, the contact with SARS-CoV-2-infected cells induces a IRF7/IFN-I/λ prioritized signaling in pDCs, while passively excluding NF-κB-mediated responses. The 'bifurcated' signaling in TLR7-activated pDCs can occur independently toward either IFN-I/λ production or NF-κB activation leading to pro-inflammatory cytokines and activation markers. This bifurcation of signaling is expected to be dependent on the sub-cellular compartment in which the TLRs encounter activating signal: activation in early endosomes induces IFN-I while activation in endolysosomes triggers NF-κB-mediated signaling **(Combes et al., 2017; Reizis, 2019)**. We previously reported that, in the context of

other viral infections (*i.e.*, Dengue, Chikungunya, Hepatitis C, Zika viruses), contact with infected cells similarly induced a IRF7/IFN-I/λ prioritized signaling in activated pDCs, as opposed to incubation of pDCs with cell-free viruses **(Assil et al., 2019; Webster et al., 2018)**. Of note, we also show that stimulation of pDCs by cell-free SARS-CoV-2 supernatants induced the upregulation of some activation markers (*e.g.*, HLA-DR, PD-L1), in accordance with other reports **(Alculumbre et al., 2018; Onodi et al., 2021),** but elicited virtually no IFN-I/λ response. We propose that the signaling downstream of TLR7, including the phosphorylation cascade might be impacted by cell polarity and physical contact with infected cells **(Olayioye et al., 2013; Saitoh et al., 2017)**. Further studies will aim at addressing this question.

Cross-regulation of immune responses.

Progression to severe COVID-19 predominates in elderly patients, advanced age being a factor suspected to aggravate disease progression and to weaken innate immunity, potentially including pDC responsiveness **(Feng et al., 2021; Jing et al., 2009)**. This is in accordance with the demographic analysis of our COVID-19 cohort, as the age-ranges were 63.5-year-old [interquartile of 48.0-73.0] and 40.5-year-old [24-57] for *Severe* and *Mild* patients, respectively. The patient history and genetic factors can explain the differential ability of pDCs from patients to mount a response against SARS-CoV-2-infected cells, as illustrated by the heterogeneous immune responses of patients, with critical anomalies in functionality of pDC in severe COVID-19. Here, a kinetic analysis performed on a COVID-19 patient that presents auto-antibodies against IFNα **(Bastard et al., 2021a; Bastard et al., 2021b; Bastard et al., 2020; Lopez et al., 2021)** show that the responsiveness of pDCs to stimulation by SARS-CoV-2-infected cells was blunted. Future study is needed to expand this interesting preliminary observation, which already indicates that the IFN-I/λ response can reinforce via a positive feedforward regulation the pDC antiviral function.

Of note, comparison of responses across patients with different COVID-19 severities suggest that pDC response to SARS-CoV-2-infected cells inversely correlates with an exacerbated inflammatory response (as illustrated by IL6 production by monocytic cells) and a basal level IFN-I/λ and inflammation activity. It is tempting to speculate that the progressive enrichment of proinflammatory cytokines in the lung micro-environment can imprint pDC responsiveness. In this scenario, an excessive elicitation of pDC would lead to their functional 'silencing'. Future study is needed to elucidate the underlining mechanism that could lead to such '*exhausted*' pDCs, as reminiscent of the findings of impaired pDC

function in a distinct infection context **(Macal et al., 2018)**. In turn, the deficit of the antiviral control at the infected site owing to *exhausted* pDCs can then feedback as fuel for uncontrolled viral replication leading to more lung inflammation. Altogether our results thus highlighted possible cross-regulation between immune cells in the course of COVID-19.

Concluding remarks: importance for SARS-COV2 and possible insight for predictive markers.

SARS-CoV-2 is a still-ongoing worldwide health threat, currently causing a significant human and economic burden and exacerbated by divergence into more severe variants. We provide compelling evidence that pDCs are a key cell type in the initiation of antiviral responses against SARS-CoV-2. Further, this study identified the failure of pDC response as critical in COVID-19 severity. Moving forward our finding shall provide guidelines for predictive biomarkers, as associated with pDC responsiveness to SARS-CoV-2 infections and background IFN-I/λ response at different stages of disease. Furthermore, strategies to boost the pDC response, and especially their recruitment to the lung, can lead to the development of potential therapeutics against pulmonary viral infections, including SARS-COV-2.

START Methods

Detailed methods are provided in the online version of this paper and include the following:

- **KEY RESOURCES TABLE**
- **CONTACT FOR REAGENT AND RESOURCE SHARING**
- **EXPERIMENTAL MODEL AND SUBJECT DETAILS**

Preparation of Viral Stocks and Infections

Cell Lines and Primary Cell Cultures

Cohort of SARS-CoV-2 infected patients.

Reagents

- **METHOD DETAILS**

Quantification of SARS-CoV-2 level in nasal swab samples of infected patients.

Analysis of IFN-I/λ signatures in blood samples of SARS-CoV-2-infected patients.

Ex-vivo stimulation of PBMCs isolated from SARS-CoV-2-infected patients and healthy donors.

Coculture experiments using isolated pDCs

Immunostaining and flow cytometry analysis

Analysis of transcriptional levels by RT-qPCR

Analysis of extracellular infectivity

Viral Spread Assay

Live imaging of coculture with spinning-disc confocal microscopy analysis

- **QUANTIFICATION AND STATISTICAL ANALYSIS**

PCA analysis

Bioinformatic analysis of the cis-acting regulatory element in the promoter

Statistical methods.

- **CONTACT FOR REAGENT AND RESOURCE SHARING**

Further information and requests for resources and reagents should be directed to and will be fulfilled by the Lead Contact, Dr. Marlène Dreux (marlene.dreux@ens-lyon.fr)

- **EXPERIMENTAL MODEL AND SUBJECT DETAILS**

Preparation of Viral Stocks and Infections.

The clinical isolate was obtained from patients referenced in the GISAID EpiCoVTM database: as BetaCoV/France/IDF0571/2020; accession ID: EPI_ISL_411218 **(Pizzorno et al., 2020)**, kindly provided by Dr B. Lina. The infectious-clone-derived mNeonGreen SARS-CoV-2 (referred to as icSARS-CoV-2-mNG) was kindly provided by Dr Pei-Yong Shi and generated by introducing mNeonGreen into ORF7 of the viral genome **(Xie et al., 2020)**. Viral stock of Influenza A Virus (Flu A/H1N1/New caledonia ; infectious titer of $\approx 10^7$ plaque forming unit (PFU)/ml) **(de Chassey et al., 2013)** was produced as previously described and kindly provided by Dr V. Lotteau (CIRI, Lyon France).

Cell Lines and Primary Cell Cultures.

SARS-CoV-2-infected cells included the human alveolar basal epithelial cell lines, Calu-3 cells (ATCC HTB-55), A549 cells (ATCC CCL-185) and NCI-H358 cells (ATCC CRL-5807), Huh7.5.1 cells **(Dreux et al., 2012)** and HEK-293 cells (ATCC CRL-1573). The A549 cells, NCI-H358 cells and HEK-293 cells were transduced to stably express the human angiotensin converting enzyme 2 (ACE2; accession number: NM_021804) using a lentiviral vector, as previously described **(Dreux et al., 2012; Rebendenne et al., 2021)**. A549 cells were maintained in Roswell Park Memorial Institute (RPMI) 1640 Medium (Life Technologies) supplemented with 10% FBS, 100 units (U)/ml penicillin, 100mg/ml streptomycin and non-essential amino acids (Life Technologies) at 37°C/5% CO_2. The NCI-H358 and Huh7.5.1 cells were maintained in Dulbecco's modified Eagle medium (DMEM) (Life Technologies) with the same supplements and 2mM L-glutamine. Calu-3 cells were maintained in DMEM/Nutrient mixture F-12 Ham (1:1) (Life Technologies) supplemented with glutaMAX, 10% FBS, 100 units (U)/ml penicillin, and 100mg/ml streptomycin. All cell were maintained at 37°C/5% CO_2.

pDCs were isolated from 450 ml of blood units obtained from adult human healthy donors and according to procedures approved by the “Etablissement Français du sang” (EFS) Committee. PBMCs were isolated using Ficoll-Hypaque density centrifugation. pDCs were

positively selected from PBMCs using BDCA-4-magnetic beads (MACS Miltenyi Biotec) and cultured as previously described **(Assil et al., 2019)**. PBMCs and pDCs were cultured in RPMI 1640 Medium (Life Technologies) supplemented with 10% FBS, 100 units (U)/ml penicillin, 100 mg/ml streptomycin, 2 mM L-glutamine, non-essential amino acids, 1 mM sodium pyruvate and 10 mM Hepes (Life Technologies) at 37°C/5% CO_2.

Cohort of SARS-CoV-2 infected patients.

The constitution of the cohort was done by the collaboration of the Hospices Civils de Lyon (HCL). This cohort consists of patient groups recognized by clinicians as: *i)* patients admitted in intensive care units for severe disease at hospital admission (*i.e.,* acute respiratory distress syndrome or severe pneumonia requiring mechanical ventilation, sepsis and septic shock) are referred to as *Severe group* and *ii)* patients with mild symptoms (*i.e.,* low-grade fever, cough, malaise, rhinorrhea, sore throat) are referred to as *Mild early group* when collected in the first two weeks and *Mild late group* for later time points. A detailed description of the patient information along with the levels of the IFN-I/III signature and viremia, as determined in blood and nasal swab samples, respectively, is provided in **Table 1 and S1**. As reference, blood samples from *healthy donors* were obtained from EFS and experimentally processed similarly. To limit the risk of inclusion of asymptotic healthy donor: *i/* part of the blood samples was collected prior to the pandemic and *ii/* for blood collected during the SARS-CoV-2 pandemic, systemic examination and questioning/interview of the donors were performed and included symptoms, prior contacts at risk and vaccination, Thus, blood samples were excluded from our study if ongoing and/or recent COVID-positivity was suspected.

Reagents.

The antibodies used for immuno-staining are listed in the **Key Resource table**. Ficoll-Hypaque (GE Healthcare Life Sciences). Other reagents included LPS, TLR3 agonist (Poly(I:C); LMW) and TLR7 agonist (R848 and Imiquimod) (Invivogen); TLR7 antagonist (IRS661, 5'-TGCTT GCAAGCTTGCAAGCA-3' synthesized on a phosphorothionate backbone; MWG Biotech); mouse anti-α_L integrin (clone 38; Antibodies Online); mouse anti-ICAM-1 (Clone LB-2 ; BD Bioscience): Arp2/3 complex inhibitor I (CK-666 ; Merck Millipore) ; Fc Blocking solution (MACS Miltenyi Biotec); Golgi-Plug, cytoperm/cytofix and permeabilization-wash solutions (BD Bioscience); IFNα and IFN*λ1/2/3* ELISA kit (PBL Interferon Source); IL6 and TNFα ELISA kit (Affymetrix, eBioscience); 96-well format

transwell chambers (Corning); IL6 and IFNλ by U-PLEX Custom Human Cytokine assay (Meso Scale Diagnostics, Rockville, MD) ; 96-Well Optical-Bottom Plates (Thermo Fisher Scientific); cell-labeling solution using CellTraceTM Violet Cell Proliferation Kit (Life Technologies ref # C34557, C34571), Live/Dead Fixable Dead Cell Stain Near-IR (Life Technologies ref #10119); Fixable Viability Dye eFluor 450 (Life Technologies); Zombie Aqua and Zombie Green Fixable Viability Kits (Biolegend); FITC Annexin V Apoptosis Detection Kit with 7-AAD (Biolegend); cDNA synthesis and qPCR kit (Life Technologies) ; poly-L-lysin (P6282, Sigma-Aldrich).

- **METHOD DETAILS**

Quantification of SARS-CoV-2 level in nasal swab samples of infected patients.

Nucleic acid extraction was performed from 0.2 mL naso-pharyngeal swabs using NUCLISENS easyMAG and amplification was performed using Biorad CFX96. Quantitative viral load was determined using four internally developed quantification standards (QS) targeting the SARS-CoV-2 N gene: QS1 to QS4 respectively at $2.5.10^6$, $2.5.10^5$, $2.5.10^4$, $2.5.10^3$ copies/mL of a SARS-CoV-2 DNA standard. These QS were controlled and quantified using the Nanodrop spectrophotometer (ThermoFisher) and Applied Biosystems QuantStudio 3D Digital PCR. In parallel, naso-pharyngeal swabs were tested using the CELL Control R-GENE kit (amplification of the HPRT1 housekeeping gene) that contains two quantification standards QS1 and QS2, at 10^4 copies/µL (50,000 cells/PCR *i.e.* $1.25.10^6$ cells/mL in our conditions) and 10^3 copies/µL (5000 cells/PCR *i.e.* $1.25.10^5$ cells/mL in our conditions) of DNA standard, respectively, to normalize the viral load according to the sampling quality.

$$Normalized\ viral\ Load[\log_{10} cp/mL] = \log_{10}\left[\frac{number\ of\ SARS\text{-}CoV\text{-}2\ copies\ per\ mL}{number\ of\ cells\ per\ mL} \times 10^6 cells\ per\ mL\right]$$

Analysis of IFN-I/λ signatures in blood samples of SARS-CoV-2-infected patients.

Transcript levels using Nanostring technology. Targeted transcripts of the IFN-I pathway included SIGLEC1, IFI27, IFI44L, IFIT1, ISG15, RSAD2, HPRT1, POLR2A and ACTB **(Pescarmona et al., 2019)**. Transcript levels were determined using RNA extracted from the patient's blood samples by Maxwell 16 LEV simply RNA Blood kits that comprised an individual DNAse treatment **(Pescarmona et al., 2019)**. Next, total RNA was eluted in 40 µL RNAse-free water and concentration was quantified by spectrophotometry using a NanoVue (Biochrom). Only 200 ng of RNA were needed to achieve IFN signature with Nanostring

technology. For the Elements system, capture (probe A) and tag (probe B) probe DNA oligos were designed by NanoString and synthesized by Integrated DNA Technologies (IDT). After hybridization at 67°C for 18-20 hours, samples were analyzed using the "High Sensitivity" protocol option on the nCounter Prep Station and counted on nCounter Digital Analyzer using maximal data resolution. Data were processed with nSolver software (NanoString Technologies, Seattle, WA), which included assessment of the quality of the runs, and combined, normalized, and analyzed in nSolver and Excel.

Normalization was performed by applying a scaling factor that normalizes the geometric mean of housekeeping genes (β-Actin; *ACTB*, hypoxanthine phosphoribosyltransferase 1; HPRT1 and RNA polymerase II subunit A ; POLR2A) for each sample and these normalized counts were used to calculate the scores, as previously reported **(Pescarmona et al., 2019).** The median of these ISG relative expression was used as an IFN score.

<u>IFNα protein measurement by Simoa technology</u>. All reagents were purchased from Quanterix (reference 100860) and loaded onto the Simoa HD-1 Analyzer (Quanterix) according to the manufacturer's instructions and using three-step assay configurations. Briefly, the beads were pelleted with a magnet to remove supernatant (SN). Following several washes, 100 uL of detector antibody were added, according to the manufacturer's instructions. The beads were then pelleted with a magnet, followed by washes and 100µL of ß–D–galactosidase (SβG) were added. The beads were washed, re-suspended in resorufin ß-D-galactopy-ranoside (RGP) solution, and loaded onto the array. The array was then sealed with oil and imaged. Images of the arrays were analyzed and AEB (average enzyme per bead) values were calculated by the software in the HD-1 Analyzer, as previously reported **(Wilson et al., 2016)**. Human plasma samples along with calibration curves were measured using the Simoa HD-1 Analyzer. The calibration curves were fit using a 4PLfit with 1/y2 weighting factor and were used to determine the concentrations of the unknown human plasma samples. This analysis was done automatically using the software provided by Quanterix with the Simoa HD-1 Analyzer.

<u>IL6, IFNλ1 and IFNγ protein measurements.</u> Concentrations were determined in patient's serum using U-PLEX Custom Human Cytokine assay (Meso Scale Diagnostics, Rockville, MD). The assays were performed according to the manufacturer's instructions with overnight incubation of the diluted samples and standards at 4°C. The electrochemiluminescence signals (ECL) were detected by MESO QuickPlex SQ 120 plate reader (MSD) and analyzed with Discovery Workbench Software (v4.0, MSD).

***Ex-vivo* stimulation of PBMCs isolated from SARS-CoV-2-infected patients and healthy donors.**

Bloods of SARS-CoV-2-infected patients and healthy donors were collected in EDTA tubes. PBMCs were freshly isolated by Ficoll-Hypaque density centrifugation followed by washing in pDC/PMBC culture medium (*i.e.*, RPMI 1640 Medium supplemented with 10% FBS, 100 U/ml penicillin, 100 mg/ml streptomycin, 2 mM L-glutamine, non-essential amino acids, 1 mM sodium pyruvate and 10 mM Hepes). PMBCs were frozen in 1mL freezing medium (10% DMSO, 90% FBS) and cryopreserved in vapor phase liquid nitrogen (>-135°C). Two hours prior to *ex vivo* stimulation, PBMCs were thawed out at 37°C rinsed with 10 mL of FCS, incubated in 40 mL of pDC/PMBC culture medium at 37C°/5% CO_2 for 30 minutes and resuspended in culture medium. 2.5x10e5 PBMCs were cocultured with 1x10e5 SARS-CoV-2-infected *versus* uninfected A549-ACE2 cells, as negative control, or were stimulated with TLR agonists [31.8 µM R848 and 42.22 µM polyI:C] for the FACS panel of mDC1/pDC analysis and LPS stimulation [2.04 µM] for the mDC2/non-mDC2/HLA-DR$^+$ CD14$^+$ panel in a final volume of 200µl in 96-well round-bottom plates incubated at 37C°/5% CO_2 for 14 to 16 hours. Cell-culture SNs were collected for quantification of cytokine levels (IFNα by ELISA/Simoa; IL6, IFNγ and IFNλ1 by U-PLEX Custom Human Cytokine assay) while cells were harvested for flow cytometry or for Nanostring analyses.

RNAs were isolated from these cells by phenol/chloroform extraction procedure as previously described **(Assil et al., 2019)**. The subsequent steps of the procedure used for Nanostring analysis on *ex-vivo* stimulated PBMCs were performed as described above for the patient blood samples.

Coculture experiments using isolated pDCs.

Unless indicated differently, 2x10e4 pDCs were cocultured with SARS-CoV-2-infected or uninfected cells as 5x10e4 or 1x10e5 cells for analysis by RT-qPCR or flow cytometry, respectively or were stimulated with 100µl of cell-free SN collected from SARS-CoV-2-infected cells. The cells were infected at MOI 0.01, 0.1, 0.02 and 0.5 for, respectively, NCI-H358-ACE2, Huh7.5.1, A549-ACE2 and Calu-3 cells for 48 hours maximum prior to collection of the cells and their SNs for coculture. As comparison pDCs were stimulated with TLR agonists [31.8 µM R848 and 42.22 µM polyI:C] in a final volume of 200µl in 96-well round-bottom plates incubated at 37C°/5% CO_2. When indicated, cells were cocultured in 96-well format transwell chambers (Corning) with a 0.4 µm permeable membrane. At the indicated time, cell-culture supernatants were collected for quantification of cytokine levels:

IFNα, IFN*λ1/2/3* (IL29/28A/28B), TNFα and IL6 using specific ELISA kit (PBL Interferon Source, Affymetrix, respectively) following the manufacturer's instructions. Cells were harvested at the indicated times for analysis by flow cytometry or RT-qPCR.

Immunostaining and flow cytometry analysis.

At the indicated times, harvested cells were resuspended using 2 mM EDTA-PBS solution for the coculture with PBMCs and 0.48 mM EDTA-PBS solution for pDC cocultures. Cells were incubated with 1 µL/mL viability marker diluted in PBS for 20 minutes at RT. After a 10-minute incubation with Fc receptor blocking reagent (MACS Miltenyi Biotec) at 4°C followed by two PBS washes, cells were stained for surface markers for 30 minutes at 4°C with antibodies diluted in staining buffer (PBS without calcium and magnesium, with 2% FBS and 2mM EDTA), followed by two PBS washes. These markers included generic lineage markers (CD3, CD19, CD20, CD56 for exclusion, and CD11c, HLA-DR for selection of cell populations), and specific markers of pDCs (CD123, BDCA-2, CD2 and Axl), mDC2 (BDCA-1), mDC1 (BDCA-3), monocytes (CD14 and CD16) and/or cell differentiation markers (CD83, CD80 and PD-L1). The references and used concentrations for the antibodies are listed in the **Key resource table**. For the identification of apoptotic and necrotic cells, surface-stained cells were labelled using FITC Annexin V Apoptosis Detection Kit with 7-AAD according to the manufacturer's instructions. Following one wash with Annexin V Binding Buffer (Biolegend), cells were fixed with 4% PFA for 30 minutes at 4°C. For intracellular-immunostaining, cells were treated with 1 µl/ml GolgiPlug solution (BD Bioscience) for 3 hours at 37°C/5% CO_2 before collection. After surface staining and fixation with cytoperm/cytofix solution (BD Bioscience) for 20 minutes at 4°C, IFNα, IL6, IFN*λ1*, and TNFα were stained by a 45-minute incubation at 4°C with antibodies diluted in permeabilization buffer (BD Bioscience ; antibodies are listed in the **Key resource table)**. Cells were then washed with permeabilization buffer and resuspended in staining buffer. Flow cytometric analysis was performed using a BD LSR Fortessa 4L. Compensation beads were used as reference for the analysis. The data were analyzed using Flow Jo software (Tree Star).

Analysis of transcriptional levels by RT-qPCR.

RNAs were isolated from cells harvested in guanidinium thiocyanate citrate buffer (GTC) by phenol/chloroform extraction procedure as described previously **(Assil et al., 2019)**. The mRNA levels of human *MXA, ISG15, IFNL, IL6, TNFA* and glyceraldehyde-3-phosphate

dehydrogenase (*GADPH*) were determined by RT-qPCR using iScript RT kit (Life Technologies) and PCR Master Mix kit (Life Technologies) for qPCR and analyzed using StepOnePlus Real-Time PCR system (Life Technologies). The sequences of the primers used for RT-qPCR are described in **Table S1**. The mRNA levels were normalized to *GADPH* mRNA levels.

Analysis of extracellular infectivity.

Infectivity titers in supernatants were determined by end-point dilution in plaque assay. Briefly, 10-fold serial dilutions of SARS-CoV-2-containing supernatants were added to 2x10e5 Vero cells seeded in 12-well plates for a 2 hour-incubation. The medium was then replaced by DMEM containing 2% FBS and 2% carboxymethylcellulose (CMC). The cytopathic effect was scored 96 hours post-infection : cells were fixed for 30 minutes with 4% PFA and colored by cristal violet solution.

For icSARS-CoV-2-mNG infection, foci were directly detected according to mNeongreen-positive cells. Briefly, 10-fold serial dilutions of icSARS-CoV-2-mNG-containing supernatants were added to 2x10e4 Vero cells seeded in 96-well plates and fixed 24 hours post-infection. GFP-expressing cells were quantified by foci counting using a Zeiss Axiovert 135 microscope.

Viral Spread Assay.

A549-ACE2 cells were transduced with lentiviral-based vector pseudotyped with VSV glycoprotein to stably express RFP, as previously reported **(Assil et al., 2019)**. After immuno-isolation, pDCs were stained with CellTrace Violet Cell Proliferation kit (Life Technologies) for 20 minutes at 37°C in the dark. Labeled pDCs were then spinned down and resuspended in pDC culture medium. 2.5x10e4 pDCs were cocultured with 2.5x10e4 icSARS-CoV-2-mNG-infected cells (infected for 24 hours prior to coculture) and with 2.5x10e4 RFP^+ uninfected cells for 48 hours at 37°C/5% CO_2. When indicated, the cocultures were treated with an anti-α_L integrin blocking antibody at 10mg/mL. After coculture, harvested cells were stained with Live/Dead Fixable Dead Cell Stain Near-IR marker for 30 minutes at RT, washed with PBS and fixed with 4% PFA for 30 minutes at 4°C. The level of viral spread from icSARS-CoV-2-mNG-infected cells (mNG^+) to uninfected cells (RFP^+) during coculture was determined by flow cytometric analysis as the frequency of infected cells (mNG^+/RFP^+ population) among the RFP^+ cell population and

similarly in RFP$^-$ populations. Flow cytometric analysis was performed using a BD LSR Fortessa 4L and the data were analyzed using Flow Jo software (Tree Star).

Live imaging of coculture with spinning-disc confocal microscopy analysis.

A549-ACE2 cells were infected with icSARS-CoV-2-mNG for 48 hours prior to coculture with pDCs. Infected cells were seeded (2x10e4cells per well) in a 96-Well Optical-Bottom Plate pre-coated with poly-L-lysine (1 hour incubation at 37°C/5% CO_2 with 8mg/mL poly-L-lysine). Isolated pDCs were stained with 0.5µM Vybrant cell-labeling solution (CM-DiI, Life Technologies) by successive incubations for 10 and 15 minutes at 37°C and 4°C respectively. After addition of pDCs to seeded infected cells, the cocultures were imaged every 30 minutes during 24 hours at magnification x10 with a BSL3-based spinning-disc confocal microscope (AxioObserver Z1, Zeiss). The cocultures were maintained at 37°C/5% CO_2 in an incubation chamber. Analyses of pDC motion were performed using projection of Z-stacks with maximal intensity (*i.e.*, about 5-to-10 selected Z-stacks per fields out of 30 Z-stacks in total). The quantification of mNeonGreen fluorescence intensity of infected cells and the duration of contacts between pDCs and infected cells were performed using Image J software package (http://rsb.info.nih.gov/ij). The calculations of pDC positions were performed using Trackmate plug-in of Image J software.

- **QUANTIFICATION AND STATISTICAL ANALYSIS**

PCA Analysis

PCA analyses were performed using the R princomp function (R version 4.1.0) with the correlation matrix approach **(Jolliffe and Cadima, 2016; Mardia et al., 1979; Sánchez, 1982; Venables and Ripley, 2002)**. All time points available for each patient with a complete dataset for any given cell type were used. The time points of the patients presenting a mild severity were discriminated between *Mild early* (≤ 15 days after estimated primo-infection) and *Mild late* (> 15 days). For each cell type, PCA analyses were performed independently for each stimulation condition with the parameters presented in the vectors plots.

Bioinformatic analysis of the cis-acting regulatory element in the promoter

For each candidate gene, we recovered the genomic nucleotide sequence spanning from 1500 nucleotides upstream, until 100~200 nucleotides downstream of the annotated Refseq transcription start site. For genes with more than one annotated transcription start site, we

collected the sequence from 1500 nucleotides upstream of the most 5' transcription start site until 100~200 nucleotides downstream of the most 3' transcription start site. The bioinformatic analyses were performed using the FIMO and AME tools available on https://meme-suite.org/meme/ **(Grant et al., 2011; McLeay and Bailey, 2010)** and the consensus sequence as follows:

NF-KB	GGGRNYYYCC
IRF7	MCGAAARYGAAAVT
IRF3	NSRRAAMGGAAACCGAAACYR
IRF1	NTTYASTTTCACTTTCDBTTT
IRF5	cCGAAACCGAAmCy
STAT1:STAT2	tyAGTTTCrkTTYCy
IRF9	AwCGAAACCGAAACy

Statistical methods

Statistical analysis was performed using R software environment for statistical computing and graphics, version 3.3.2.

For quantifications by ELISA, RT-qPCR and flux cytometry analyses of the levels of cytokines, ISG and cell surface markers, the statistical analyses were performed using one-way ANOVA on ranks (Kruskal−Wallis rank sum test). When the test was considered significant (p-values ≤ 0.05), we used the Tukey Kramer (Nemenyi) pairwise test as *post hoc* test for multiple comparisons of mean rank sums to determine which contrasts between individual experimental condition pairs were significant.

Of note, for each independent experiment preformed using PBMCs isolated from SARS-CoV-2 infected patients, the same procedures and analyses were done in parallel using different *healthy* donors, as references (**Figure 2, S2, 3**). Likewise, all independent experiments of cocultures with PBMCs or pDCs were performed using distinct *healthy* donors as reference (**Figure 1, S1, 4, S4, 5, S5, 6**). To test difference between the patients groups in the Flow cytometry analysis of the biomarker the different cell population (**Figure 3**) , we used the Beta regression model with the logit link function from the R 'betareg" package, which is the suitable statistical approach for modeling continuous response Y variables that vary in the open standard unit interval (0, 1). Beta regression being unable to model in case Y contains exactly 0 or 1 values, Y data was transformed to Y' as following :

$Y' = (Y * (n - 1) + 0.5)/n$

where n is the number of patients in all compared groups.

For the quantification by flow cytometry analysis of the viral spread of the icSARS-CoV-2-mNG SARS-CoV-2 molecular clones from RFP^- cells to RFP^+ cells (initially uninfected)

(**Figure 5E-F**) and for quantification of data from the live-imaging analysis using spinning-disk confocal microscopy analysis (**Figure 6**), the statistical analyses were performed using one-way ANOVA followed by Tukey multiple comparisons of means.
The set of Figures was prepared using PRISM software.

Acknowledgments

We thank Dr B. Lina for kindly provided the clinical isolate of SARS-CoV-2 (CIRI, Lyon, France); Dr Pei-Yong Shi for the infectious-clone-derived mNeonGreen SARS-CoV-2 (University of Texas Medical Branch, Galveston, US); Dr V. Lotteau (CIRI, Lyon, France) for viral stock of the influenza A virus; Dr C. Goujon for the ACE2-Lentiviral construct (Institut de Recherche en Infectiologie de Montpellier, IRIM, France) and Dr F.V. Chisari (Scripps Research Institute, La Jolla, CA) for the Huh7.5.1 cells. We are grateful to Drs Y. Jaillais, A Marçais, B. Webster, S Assil, P.Y Lozach and A. Bosseboeuf for critical reading of the manuscript and to our colleagues for their encouragement and help. We thank the technical assistance of the staffs of PLATIM and AniRA-cytometry facilities – SFR Biosciences Lyon, Gerland (UMS3444/US8) for imaging and FACS analyses. We acknowledge the contribution of the EFS Confluence-Lyon. This work was supported by grants from the *Agence Nationale de la Recherche* (ANRJCJC-iSYN); the *Fondation pour le recherche médicale* (FRM ; ANR Flash COVID-19) ; the *Agence Nationale pour la Recherche contre le SIDA et les Hépatites Virales* (ANRS – N21006CR and N19017CR) ; the *UDL/ANR IA ELAN ERC* (G19005CC); and *fondation FINOVI* (AO11 - Collaboration); from EU H2020 ZIKAlliance . PhD fellowships for S.R. and G.J. are respectively sponsored by ANRS and Université Lyon 1 ‘*Contrats doctoraux Lyon 1 dédiés à l'International*’.

Figure legends

Figure 1. pDCs are the main IFNα producers in response to contact with SARS-CoV-2-infected cells. Cells were infected by SARS-CoV-2 (indicated as +) or not (indicated as -) two days prior to coculture with PBMCs, pDC-depleted PBMCs and isolated pDCs. Infected cell types included the human alveolar basal epithelial cell lines *i.e.*, Calu-3, A549 cells and NCI-H358 cells (transduced to stably express ACE2, referred to as A549-ACE2 and NCI-H358-ACE2 cells, respectively) and Huh7.5.1 cells, as indicated. Statistical analyses of the results were performed using Wilcoxon rank-sum test and and p-values were calculated with Tukey and Kramer test. The significant contrasts are indicated when p-values are: ≤0.05; * and ≤0.005; **. **A-B.** Quantification of IFNα in the supernatants (SNs) of PBMCs, pDC-depleted PBMCs (indicated as $PBMC^+$/pDC-) and isolated pDCs (PBMC-/pDC^+) cocultured with either SARS-CoV-2-infected or uninfected Calu-3 cells (**A**) or A549-ACE2 cells (**B**), or treated with 100µl of cell-free SNs collected from SARS-CoV-2-infected cells. Viral titers of SARS-CoV-2: SN≈2.5×10^5 foci forming units (ffu)/ml, MOI ≈ 1/pDCs. Arrows indicate results below the detection threshold of the IFNα ELISA (*i.e.*, 12.5 pg/ml). Of note, each dot represents one independent experiment (n=4-9) performed distinct healthy donors (and similarly for all experiments presented in the other Figures (see material and methods section). Error bars represent the means ± standard deviation (SD); ind./cocult. = induction/coculture **C-D.** Quantification by flow cytometry of the frequency of cells positive for the indicated type of IFN (**C**) and the differentiation markers, CD83 and PD-L1 (**D**) in cell populations gated as pDC (left bars; *i.e.*, $live^+$ cells, $CD11c^-$, $CD123^+$) and non-pDC PBMCs (right bars; live $cells^+$ $CD11c^+$, $CD123^-$) (see gating strategies in **Supplementary Figure S1A**). PBMCs were cocultured with SARS-CoV-2-infected or uninfected A549-ACE2 cells or treated with TLR agonists [31.8 µM R848 and 42.22 µM polyI:C] for 14 to 16 hours. Means ± SD; Dots represent n=10-11 independent experiments/distinct healthy donors. **E-F.** Quantification of IFNα in SNs of pDCs cocultured with the indicated cell types infected or not by SARS-CoV-2. pDC were cultured with infected cells, either in direct contact (coculture) or physically separated by the semi-permeable membrane of transwell (TW), or treated with SN from the corresponding SARS-CoV-2-infected cells. IFNα concentration was also determined in the SN of SARS-CoV-2-infected cells cultured without pDC (no pDC). Arrows indicate results below the detection threshold of the IFNα ELISA (*i.e.*, 12.5 pg/ml). **G.** Quantification of IFNα in SN of pDCs cocultured with SARS-CoV-2-infected cells and treated or not with blocking antibodies against α_L-integrin and ICAM-1 at 10 µg/mL. **H.**

Quantification of IFNα in SNs of pDCs cocultured with A549-ACE2 cells or Calu-3 infected or not by SARS-CoV-2. Means ± SD; Dots represent distinct donors in independent experiments, as n=11 and n=15 for A549-ACE2 and Calu-3 cells, respectively.

Supplementary Figure 1. Assessment of pDC response and their non-productive infection by flow cytometric analysis, related to Figure 1. A-C. PBMCs, PBMCs depleted of pDCs pDC isolated from healthy donors were cocultured with SARS-CoV-2-infected or uninfected A549-ACE2 cells or treated with agonists as in **Figure 1C-D** for 14-to-16 hours. **A.** Representative flow cytometric analysis of pDC gating strategy from PBMCs: pDCs defined as singulets$^+$ live cells$^+$ CD11c$^-$ CD123$^+$ and non-pDC PBMCs as singulets$^+$ live cells$^+$ CD11c$^+$CD123$^-$. **B.** Frequency of IFNλ1 positive cells in populations gated as pDCs (left bars) non-pDC PBMCs (right bars) as shown in panel **A**. Means ± SD; n=10-11 independent experiments using distinct healthy donors. **C-D.** Quantification of IFNα in SNs of pDCs cocultured with the indicated cell types infected or not by SARS-CoV-2. pDC were cultured with infected cells, either in direct contact (coculture) or physically separated by the semi-permeable membrane of transwell (TW), or treated with SN from the corresponding SARS-CoV-2-infected cells. IFNα concentration was also determined in the SN of SARS-CoV-2-infected cells cultured without pDC (no pDC). Arrows indicate results below the detection threshold of the IFNα ELISA (*i.e.*, 12.5 pg/ml). **E.** In parallel experiments, treatment of pDCs with TLR7 agonist imiquimod (IMQ, 20 µM) in coculture *versus* transwell settings served as positive control. Means ± SD; n=3-9 independent experiments. **F-H.** Quantification of IFNα in SN of pDCs cocultured with SARS-CoV-2-infected cells and treated or not with blocking antibodies against α_L-integrin and ICAM-1 at 10 µg/mL (**F**) or ARP2/3 inhibitor (CK-666) at the indicated concentrations (**G**), or with TLR7 inhibitor (IRS661; 0.35 µM, **H**). Means ± SD; Dots represent n=4-5 independent experiments. **I**. A549-ACE2 cells were infected by icSARS-CoV-2-mNG for 24 hours prior to coculture with isolated CTV-stained pDCs and/or RFP$^+$A549-ACE2 uninfected cells for 48 hours. Viral transmission from icSARS-CoV-2-mNG-infected cells to pDCs *versus* RFP$^+$A549-ACE2-uninfected cells was assessed by flow cytometry. Results are expressed as the percentage of infected cells (mNG$^+$) in the living cell populations gated as pDCs/CTV$^+$ and CTV$^-$/RFP$^+$ cells. Means ± SD; dot plots are representative of n=4-5 independent experiments.

Figure 2. Innate responsiveness in different hematopoietic cell types issued from infected patients with various COVID severities. PBMCs issued from the indicated groups

of patients (*i.e., healthy donors, Severe, Mild early, Mild late*, see description of the patients in **Table 1** and **S1**, and Material and Methods section) were cocultured for 14-16 hours with SARS-CoV-2-infected or uninfected A549-ACE2 cells, or treated with agonists [31.8 µM R848 and 42.22 µM polyI:C or 2.04 µM LPS]. Upper panels show PCA analysis in cell populations gated as pDCs (**A**), mDC1 (**B**), mDC2 (**C**) and HLA-DR$^+$ CD14$^+$ (**D**). Clustering of the groups of patients was performed by combining the detection of multiple cell surface expressed-differentiation markers and intracellular cytokines. Each dots represent one individual patient sample. Lower panels show the eigen vectors that represent the first and second main components, with indication of the percentage of the variance explained by each principal component.

Supplementary Figure 2. Response in blood of COVID-19 patients and by their PBMCs to ex vivo stimulation by SARS-CoV-2-infected cells *versus* agonist, related to Figure 2. A. Kinetic analysis of cytokine profile of *Severe* and *Mild* COVID-19 patients. Determination of the IFN score (Nanostring technology) in whole blood as well as secreted IFNα (Simoa technology), IFNλ1 and IFNγ (U-PLEX Custom Human Cytokine assay) in plasma, at the indicated time-points. **B.** PBMCs issued from the indicated groups of patients *(Healthy donors, Severe, Mild early, Mild late*, listed in **Table 1 and S1**) were cocultured for 14-16 hours with SARS-CoV-2-infected or uninfected A549-ACE2 cells or treated with agonists as in **Figure 2**. **B.** Gating strategies for mDC1 and pDC/non-pDC (upper panels), and mDC2/non-mDC2/HLA-DR$^+$ CD14$^+$ (lower panels).

Figure 3. pDC responsiveness to SARS-CoV-2-infected cells is impaired in infected patients. PBMCs issued from the indicated groups of patients (*i.e., healthy donors, Severe, Mild early, Mild late*, see description of the patients in **Table 1** and **S1**, and Methods section) were cocultured for 14-16 hours with SARS-CoV-2-infected or uninfected A549-ACE2 cells or treated with agonists. **A-E.** Quantification by multiparametric flow cytometry of the frequency of pDCs as IFNα$^+$/IFNα^{hi} (**A**) IFNλ1$^+$ (**B**) and the differentiation markers, CD83, CD80, PD-L1 (**C-E**) in the cell population gated as pDCs (see gating strategies in **Supplementary Figure 2**). **F-G.** Quantification of the frequency of cells positive for IFNλ1 in populations gated as mDC1 (**F**) and IL6 in populations gated as HLA-DR$^+$ CD14$^+$ monocytes mDC2 and non-mDC2 (**G**), see gating strategies in **Supplementary Figure 2B**. The numbers of included patient samples are listed in the **Table 1** and **S1 (**Means ± SD**)**. **H.** Kinetic analysis of the pDC IFNα$^+$ response to the stimulation in *Mild* patients (left panel),

Severe patients (right panel) and *healthy* donors (right side of the right panel). Dots for a severe patient, who had anti-IFNα antibody detected in the blood (see description in **Table 1,** legend) is represented by cercles with yellow-center. Results are presented in intervals in weeks post-onset of the symptoms defined according to week 1 = [1-8]; 2 =]8-15]; 3 =]15-22]; 4 =]22-30].

Figure 4. SARS-CoV-2-infected cells induce pDC maturation and phenotypic diversification. Human pDCs isolated from healthy donors were cocultured with SARS-CoV-2-infected (+) or uninfected (-) A549-ACE2 or Calu-3 cells (indicated as 'cells'), or were stimulated with 100µl of cell-free SN collected immediately prior coculture from the corresponding SARS-CoV-2-infected cells (viral titers ≈ 2.5×10^5 ffu/ml - MOI ≈1/pDCs), or were stimulated with influenza virus (flu; viral titers ≈ 10^7 pfu/ml - MOI ≈ 0.5/pDCs), R848/polyI:C (R/p) or imiquimod (IMQ) for 14-16 hours (stim = stimulation; unst = unstained). **A-F** Quantification by flow cytometry of HLA-DR Geomean (**A**) or the frequency of pDCs positive for CD70 (**B**), PD-L1 and/or CD83 (**C**), CD2 (**D**), PD-L1 and/or CD80 (**E**), PD-L1 and/or CD83 among mTRAIL$^+$ pDCs (**F**) determined in gated pDCs (live cells$^+$ singulets$^+$ CD123$^+$ BDCA2$^+$, see gating strategy in **Supplementary Figure 4A**). **G**. SARS-CoV-2-infected (+) or uninfected (-) A549-ACE2 or Calu-3 cells were cultured alone (i.e., no pDC) or cocultured with pDCs for 14-16 hours. Quantification by flow cytometry of the frequency of gated A549-ACE2 and Calu-3 cells positive for Annexin V and/or 7-AAD. **H.** icSARS-CoV-2-mNG-infected A549-ACE2 were cultured alone (no pDC) or cocultured with pDCs in the presence or absence of anti-$_{\alpha L}$integrin blocking antibody for 48 hours. Quantification by flow cytometry of the frequency of living cells using live-dead marker in the gated pDCs (stained with CellTraceTM Violet prior to coculture) and infected cells/non-pDC. Bars represent means ± SD; n=3-5 independent experiments using distinct healthy donors. Each dot in panels **A-B, D-E** represents one independent experiment. The data were analyzed using Kruskal-Wallis Global test and p-values were calculated with Tukey and Kramer test; * ≤0.05 and ** ≤0.005.

Supplementary Figure 4. Activation profile and diversification of pDCs in response to coculture with SARS-CoV-2-infected cells, as compared to synthetic agonist stimulation, related to Figure 4. Purified human pDC were cocultured with uninfected (-) or SARS-CoV-2-infected (+) A549-ACE2 or Calu-3 cells, or cell-free SN collected from SARS-CoV-2-infected cells (at the time of coculture – 48 hours of infection prior to coculture) or were

stimulated (stim) with influenza virus (flu), R848/polyI:C (R/p) or imiquimod (IMQ) for 14-16 hours, as described in Figure 4. **A.** Gating strategies used to determine the activation profile and diversification of pDCs. Dot plots showing the expression of CD70, PD-L1, CD83, CD80, IFNα, TNFα and IFNλ1 are representative of n=3-5 independent experiments. **B-C.** Quantification by flow cytometry of the frequency of PD-L1, CD83 positivity in $CD2^{hi}$ and $CD2^{low}$ subsets (**B**) and CD2, CD5 and AXL subsets (**C**), determined in gated pDCs. Bars represent means ± SD; n=3-5; The data were analyzed using Kruskal-Wallis Global test and p-values were calculated with Tukey and Kramer test; ns: p >0,05; *p<0,05; **p<0,005.

Figure 5. Cell-cell contact sensing of SARS-CoV-2-infected cells by pDCs induces a robust production of IFN-I/λ and other cytokines leading to the inhibition of viral spread. Human pDCs isolated from healthy donors were cocultured with SARS-CoV-2-infected (+) or uninfected (-) cells (panels **A-G**), or were incubated with 100µl of cell-free SN collected immediately prior to coculture from the corresponding SARS-CoV-2-infected cells (panels **B-E**), or were stimulated by influenza virus or agonists (panels **D and E**) (as in **Figure 1 and 4**). **A**. Quantification of the induction of ISG (*mxA*, *isg15*), type III IFN (*ifn*λ1) and pro-inflammatory cytokines (*il6*, *tnfA*) mRNAs in SARS-CoV-2-infected or uninfected A549-ACE2, Calu3, Huh7.5.1 or 293-ACE2 cells cultured with (pDC) or without pDC (no pDC) by RT-qPCR. Means ± SD; n=3-8 independent experiments using distinct healthy donors; statistical analysis using Kruskal-Wallis Global test; p-values as * ≤0.05, ** ≤0.005 and *** ≤0.0005 (Tukey and Kramer test). **B-C.** Quantification of IFNλ1/2/3 (**B**) and TNFα (**C**) in SN of pDCs cocultured with SARS-CoV-2-infected cells [Cocult] versus SN, as indicated. Bars represent means ± SD; n=3-14 (left panel) n=2-4 (right panel) independent experiments using distinct healthy donors. **(D-E)** Quantification by flow cytometry of the frequency of pDCs positive for IFNα and/or TNFα (**D**) and IFNα and/or IFNλ1 (**E**). Bars represent means ± SD; n=3-5 independent experiments using distinct healthy donors. **F-G.** A549-ACE2 cells were infected by icSARS-CoV-2-mNG for 24 hours and then cocultured with isolated pDCs for 48 hours. Cocultured cells were treated or not with anti-α_L integrin blocking antibody (10 µg/mL). Viral transmission from icSARS-CoV-2-mNG+-infected cells to RFP+ uninfected cells in cocultures with pDC or without pDCs (no pDC) was quantified by flow cytometry (**F**) and representative dot plots (**G**). Results are expressed as the percentage of cells positive for mNeonGreen (mNG^+) in the RFP^+ (red numbers) and RFP^- (green numbers) cell populations. Means ± SD; n=4-5 independent experiments.

Supplementary Figure 5. Cell-cell contact sensing of SARS-CoV-2-infected cells by pDCs induces a robust production of IFN-I/λ and other cytokines, related to Figure 5. Human pDCs isolated from healthy donors were cocultured with SARS-CoV-2-infected (+) or uninfected (-) cells, or were incubated with 100µl of cell-free SN collected immediately prior to coculture from the corresponding SARS-CoV-2-infected cells or were stimulated by influenza virus or agonists, as in **Figure 5D-E**. Quantification by flow cytometry of the frequency of pDCs positive for IFNα and/or TNFα in regard to their diversification as PD-L1- and/or CD80-positive cells (**A**) and IFNα and/or IFNλ1 in regard to positivity for CD2 (**B**). Bars represent means ± SD; n=3-5 independent experiments using distinct healthy donors.

Figure 6. Targeted antiviral activity of pDCs toward SARS-CoV-2-infected cells. Live imaging of coculture of icSARS-CoV-2-mNG-infected cells with pDCs (CM-DiI stained) by spinning-disk confocal analysis. A549-ACE2 cells were infected by icSARS-CoV-2-mNG for 48h prior to coculture with pDCs. **A**. Representative time-sequence of pDCs (red), tracked using motion automatic tracking plug-in in image J (white line) in contact with icSARS-CoV-2-mNG-infected cells (green arrow). The time points when pDCs are in contact with infected cells are framed in grey. Bottom panels show same imaging of the seven last time points with enhanced fluorescence signal. **B-C**. Calculation of mNeongreen fluorescence intensity over time in individual icSARS-CoV-2-mNG-infected cells cocultured with pDCs: in contact (green curves) *versus* not in contact (blue curves) with pDCs (**B**), and as control/reference, in simultaneously recorded cultures of icSARS-CoV-2-mNG-infected cells without pDC (**C**), using area integrated intensity and mean value (quantification tools in Image J). The time point corresponding to the onset/start of contact is indicated by a red dot. The time point when the contact stated is indicated by red dots. The results are presented as the mNeongreen fluorescence intensity at the indicated time relative to time 0 of record set to 1; n= 5 individually recorded cells analyzed per condition from one representative experiment (and n=10-12 in other experiments). **D.** Violin plot representation of the decrease of mNeongreen fluorescence intensity (percentage) in icSARS-CoV-2-mNG-infected cells in the indicated conditions. Each dot represents one infected cell (n=118); 4 independent experiments. **E.** Violin plot representations of the contact duration between icSARS-CoV-2-mNG-infected cells and pDCs leading to control of viral replication, defined as drop of fluorescence intensity > 50% relative to the initial mNG fluoresent intensity (+) or not (-). **F.** Violin plot representations of time-lag between the onset of pDC contact and the drop of mNeongreen

fluorescence intensity defined as >50% of the initial fluorescence intensity. Each dot represents one individual icSARS-CoV-2-mNG-infected cells in contact with pDCs n=50 (**E**) and n=25 (**F**) from 4 independent experiments.

	Mild COVID-19 n=6	Severe/Critically-ill COVID-19 n= 6*
Demographics		
Age, median [IQR]	40.5 [24-57]	63.5 [48.0-73.0]
Sex		
Male, n (%)	2 (33)	4 (67)
Female, n (%)	4 (67)	2 (33)
BMI (kg/m²)	23 [17-27]	35.5 [28-49]
Clinical characteristics		
Delay between symptom onset and ICU admission, day median [IQR]	N/A	8 [3-26]
ICU length of stay, day median (min-max)	N/A	45 [23-92]
Mortality, n (%)	0 (0)	4 (67)
Auto-ab anti IFN-I, n (%)	0 (0)	1 (17)

Table 1. Demographical and clinical characteristics of health care workers (HCWs) with mild COVID-19 symptoms and severe/critically-ill COVID-19 patients. All laboratory data were recorded at recipient inclusion. Abbreviations: BMI; Body mass index, IQR; Interquartile; N/A; not applicable, ICU; intensive care unit.
* one of the severe/critically-ill COVID-19 patients was detected as positive for IFNα:
Detection using an anti-IFNα antibody - Human ELISA Kit (Thermo-fisher; ref. BMS217)
Results > 1000 ng/mL (detection in non-positive individual is < 34 ng/mL)
Detection > 1000 ng/mL associates with neutralizing antibody.

	information patients		Viral load				Cytokinic level in the blood of patients				
group	ID	day post symptom	Ct SARS N	log10 cp/ml	log10 copies /10^3 cell	Results	IFNα fg/ml	IFN score	IFNλ1 pg/mL	IL6 pg/mL	IFNγ pg/mL
Mild patients	P41-01	4	18.81	7.11	5.1	Positive	5919.0	149.96	38.26	/	41.17
	P41-02	11	27.56	4.62	2.7	Positive	2267.0	71.71	15.64	/	149.17
	P41-03	18	34.16	2.45	0.6	Positive	6.6	2.61	7.76	0.48	13.87
	P41-04	25	37.23	0.00	ND	Positive	/	1.56	2.90	0.27	9.98
	G38-01	1	23.37	5.72	3.4	Positive	7382.0	26.39	40.91	/	31.55
	G38-02	8	23.22	6.00	3.9	Positive	53.3	2.8	6.24	/	11.65
	G38-03	15	29.95	3.96	1.6	Positive	0.0	2.35	8.82	1.56	9.85
	G38-04	22	23.3	5.73	3.8	Positive	/	ND	0.85	0.90	4.84
	G17-01	4	21.65	6.24	3.9	Positive	245.0	39.02	7.60	/	151.88
	G17-02	10	/	/	/	/	9.2	4.46	9.23	/	15.36
	G17-03	19	/	/	/	/	0.0	3.36	3.37	0.23	94.97
	G17-04	25	/	/	/	/	/	1.86	0.85	0.90	4.84
	G17-05	183	/	/	/	/	/	/	2.19	0.71	13.85
	A30-01	1	23.53	5.67	4.2	Positive	3683.0	123.66	8.83	1.06	13.78
	A30-02	8	26.59	4.79	2.8	Positive	173.2	27.65	4.32	0.60	13.46
	A30-03	14	ND	1.65	-0.5	Positive low	0.0	1.41	2.16	0.33	5.61
	A30-04	22	ND	ND	ND	Negative	ND	1.68	2.67	0.76	6.45
	A30-05	183	/	/	/	/	/	/	1.84	0.24	3.47
	L175-01	1	16.73	7.6	6.8	Positif	2.9	173.9	24.17	0.64	108.69
	L175-02	8	/	/	/	/	25.2	18.27	3.58	0.47	18.12
	L175-03	13	38.55	0.87	ND	Positive low	/	3.71	2.14	0.32	8.75
	L175-04	20	/	/	/	/	/	2.74	2.01	0.27	9.73
	L175-05	183	/	/	/	/	/	/	1.89	0.32	7.71
	P29-01	2	22.73	5.91	3.9	Positive	774.0	76.76	9.04	/	203.40
	P29-02	9	/	/	/	/	4.2	2.63	3.79	/	9.27
	P29-03	16	/	/	/	/	1.4	2.3	1.97	0.39	13.34
	P29-04	23	/	/	/	/	/	2.07	/	/	/
	P29-05	30	/	/	/	/	/	/	2.32	0.27	7.88
	P29-06	183	/	/	/	/	/	/	2.72	0.30	11.62
Severe patients	C-01	27	30.8	/	/	Positive	22.4	0.9	3.69	11.09	ND
	C-02	37	ND	/	/	Negative	13.3	< 0.4	1.34	0.86	4.59
	B-01	9	/	/	/	Positive	0.0	2.7	21.99	/	48.12
	B-02	11	/	/	/	Positive	0.0	0.6	14.29	/	11.37
	B-03	15	/	/	/	Positive	0.0	0.8	12.76	/	5.07
	H-01	15	25.5	/	/	Positive	0.0	0.5	9.00	107.49	15.27
	H-02	18	pos	/	/	Positive	28.0	1	7.83	138.92	8.82
	H-03	20	pos	/	/	Positive	16.7	0.9	6.02	260.51	79.26
	F-01	12	35.7	/	/	Positive	0.8	2.37	/	/	/
	F-02	28	ND	/	/	Negative	5.6	0.53	/	/	/
	F-03	35	ND	/	/	Negative	0	0.39	/	/	/
	O-01	8	19.7	/	/	Positive	1025	39.89	/	/	/
	O-02	16	21.1	/	/	Positive	0	1.19	2.46	1.63	8.68
	O-03	23	32.7	/	/	Positive	0	1.53	7.90	6.31	39.75
	O-04	30	ND	/	/	Negatif	3.9	0.87	11.05	9.18	50.80
	R-01	36	32.1	/	/	Positive	7.5	1.1	/	/	/
	R-02	43	ND	/	/	Negative	7.3	0.74	3.02	18.83	7.36
	R-03	50	ND	/	/	Negative	11	2.28	5.04	2.44	16.63

Table S1. Viral load and cytokinic profiles of SARS-CoV-2 infected patients with mild and severe/critically-ill COVID-19. Viral load in nasal swab determined by qPCR relative to the volume and number of cells. Abbreviations: ND ; not detected, / ; not determined.

Gene	Forward Primer	Reverse Primer
MXA	ACAGGACCATCGGAATCTTG	CCCTTCTTCAGGTGGAACAC
ISG15	GACAAATGCGACGAACCTCT	CGGCCCTTGTTATTCCTCA
IFNλ1	TCCTAGACCAGCCCCTTCA	GTGGGCTGAGGCTGGATA
IL6	GTCAGGGGTGGTTATTGCAC	AGTGAGGAACAAGCCAGAGC
TNFα	AGATGATCTGACTGCCTGGG	CTGCTGCACTTTGGAGTGAT
GAPDH	AGGTGAAGGTCGGAGTCAACG	TGGAAGATGGTGATGGGATTTC

Table S2. Primer sequences for quantitative real-time PCR

		consensus sequence for regulators related to:									
		IRF/IFN-I							NF-κB		
name in the text	**Accession number**	**IRF 7**	**IRF 3**	**IRF 1**	**IRF 5**	**STAT1: STAT2**	**IRF 9**	**IRF 8**		**https://www.bu.edu/nf-kb/gene-resources/target-genes/ and http://www.interferome.org/interferome/home.jspx**	**references**
IFNα1	NM_024013.3	2	2	6	0	0	0	0	0	N.D for NF-κB	
IFNα2	NM_000605.4	0	0	1	0	0	0	0	0	N.D for NF-κB	(Marie et al., 1998)
IFNα4	NM_021068.3	0	0	3	0	0	0	0	0	N.D for NF-κB	(Marie et al., 1998)
IFNb1	NM_002176.4	1	2	2	1	1	0	0	0	*not directly demontstrated - likely for B lymphocytes and fibroblasts	(Hiscott et al., 1989; Lenardo et al., 1989)
ISG15	NM_005101.4	1	5	6	2	4	4	2	1	N.D for NF-κB	
*MxA**	NM_001144925.2	1	3	4	4	7	2	1	8	*kB site in the promoter but has not been shown to be controlled by NF-kB or the gene expression is associated with increased NF-kB activity	(Gerardin et al., 2004)
IFNλ1 IL28A	NM_172140.2	1	2	2	0	1	2	0	0	N.D for NF-κB	
IFNλ2 IL28B	NM_172138.2	1	1	4	1	1	0	0	1	N.D for NF-κB	
IFNλ3 IL29	NM_001346937.2	1	2	2	1	2	0	0	1	N.D for NF-κB	
CD70	NM_001252.5	0	0	1	0	0	0	0	2	NF-kB site: NFKAPPAB & NFKAPPAB50	
CD83	NM_001040280.3	0	0	0	0	0	0	0	4	Target Genes of NF-kB	(Berchtold et al., 2002; McKinsey et al., 2000)
TRAIL	NM_003810.4	0	2	4	0	2	0	0	1	Target Genes of NF-kB	(Baetu et al., 2001; Matsuda et al., 2005)
TNFα	NM_000594.4	0	2	1	1	1	1	1	2	Target Genes of NF-kB	(Collart et al., 1990; Shakhov et al., 1990)
HLA-DRa	NM_019111.5	0	0	1	0	0	1	1	0	N.D for NF-κB	
IL6	NM_001371096.1	1	0	3	1	0	1	0	1	Target Genes of NF-kB	(Libermann and Baltimore, 1990; Shimizu et al., 1990; Son et al., 2008)
CD80	NM_005191.4	0	0	2	0	0	0	0	0	Target Genes of NF-kB	(Fong et al., 1996; Zhao et al., 1996)
PD-L1 (CD274 B7-H1)	NM_014143.4	3	2	2	1	3	2	1	0	Target Genes of NF-kB	(Antonangeli et al., 2020; Lee et al., 2005)

Table S3: Regulation of the selected biomarkers by the IRF/IFN-I *versus* NF-κB pathways. The identification of cis-acting regulatory elements in promotor of the set of analyzed markers was performed as described in the Method section, using the FIMO and AME tools available on https://meme-suite.org/meme/ (Grant et al., 2011; McLeay and Bailey, 2010).

Additional searches were performed using website, as reference: https://www.bu.edu/nf-kb/gene-resources/target-genes/ and http://www.interferome.org/interferome/home.jspx and the supplemental source/retrieved publications are indicated.
Abbreviations: ND; not determined.
Of note, IRF7 and VAF transcription factors binds to IFN-alpha and IFN-beta promoter regions and induce the IFN-alpha and beta mRNA.

References

Abbas, A., Vu Manh, T.P., Valente, M., Collinet, N., Attaf, N., Dong, C., Naciri, K., Chelbi, R., Brelurut, G., Cervera-Marzal, I.*, et al.* (2020). The activation trajectory of plasmacytoid dendritic cells in vivo during a viral infection. Nature immunology *21*, 983-997.

Achard, C., Guillerme, J.B., Bruni, D., Boisgerault, N., Combredet, C., Tangy, F., Jouvenet, N., Gregoire, M., and Fonteneau, J.F. (2017). Oncolytic measles virus induces tumor necrosis factor-related apoptosis-inducing ligand (TRAIL)-mediated cytotoxicity by human myeloid and plasmacytoid dendritic cells. Oncoimmunology *6*, e1261240.

Alculumbre, S.G., Saint-Andre, V., Di Domizio, J., Vargas, P., Sirven, P., Bost, P., Maurin, M., Maiuri, P., Wery, M., Roman, M.S.*, et al.* (2018). Diversification of human plasmacytoid predendritic cells in response to a single stimulus. Nature immunology *19*, 63-75.

Antonangeli, F., Natalini, A., Garassino, M.C., Sica, A., Santoni, A., and Di Rosa, F. (2020). Regulation of PD-L1 Expression by NF-kappaB in Cancer. Front Immunol *11*, 584626.

Asano, T., Boisson, B., Onodi, F., Matuozzo, D., Moncada-Velez, M., Maglorius Renkilaraj, M.R.L., Zhang, P., Meertens, L., Bolze, A., Materna, M.*, et al.* (2021). X-linked recessive TLR7 deficiency in ~1% of men under 60 years old with life-threatening COVID-19. Sci Immunol *6*.

Assil, S., Coleon, S., Dong, C., Decembre, E., Sherry, L., Allatif, O., Webster, B., and Dreux, M. (2019). Plasmacytoid Dendritic Cells and Infected Cells Form an Interferogenic Synapse Required for Antiviral Responses. Cell host & microbe *25*, 730-745 e736.

Baetu, T.M., Kwon, H., Sharma, S., Grandvaux, N., and Hiscott, J. (2001). Disruption of NF-kappaB signaling reveals a novel role for NF-kappaB in the regulation of TNF-related apoptosis-inducing ligand expression. J Immunol *167*, 3164-3173.

Bastard, P., Gervais, A., Le Voyer, T., Rosain, J., Philippot, Q., Manry, J., Michailidis, E., Hoffmann, H.H., Eto, S., Garcia-Prat, M.*, et al.* (2021a). Autoantibodies neutralizing type I IFNs are present in ~4% of uninfected individuals over 70 years old and account for ~20% of COVID-19 deaths. Sci Immunol *6*.

Bastard, P., Orlova, E., Sozaeva, L., Levy, R., James, A., Schmitt, M.M., Ochoa, S., Kareva, M., Rodina, Y., Gervais, A.*, et al.* (2021b). Preexisting autoantibodies to type I IFNs underlie critical COVID-19 pneumonia in patients with APS-1. The Journal of experimental medicine *218*.

Bastard, P., Rosen, L.B., Zhang, Q., Michailidis, E., Hoffmann, H.H., Zhang, Y., Dorgham, K., Philippot, Q., Rosain, J., Beziat, V.*, et al.* (2020). Autoantibodies against type I IFNs in patients with life-threatening COVID-19. Science (New York, N.Y *370*.

Benard, A., Jacobsen, A., Brunner, M., Krautz, C., Klosch, B., Swierzy, I., Naschberger, E., Podolska, M.J., Kouhestani, D., David, P.*, et al.* (2021). Interleukin-3 is a predictive marker for severity and outcome during SARS-CoV-2 infections. Nat Commun *12*, 1112.

Berchtold, S., Muhl-Zurbes, P., Maczek, E., Golka, A., Schuler, G., and Steinkasserer, A. (2002). Cloning and characterization of the promoter region of the human CD83 gene. Immunobiology *205*, 231-246.

Blanco-Melo, D., Nilsson-Payant, B.E., Liu, W.C., Uhl, S., Hoagland, D., Moller, R., Jordan, T.X., Oishi, K., Panis, M., Sachs, D.*, et al.* (2020). Imbalanced Host Response to SARS-CoV-2 Drives Development of COVID-19. Cell *181*, 1036-1045 e1039.

Blasius, A.L., Arnold, C.N., Georgel, P., Rutschmann, S., Xia, Y., Lin, P., Ross, C., Li, X., Smart, N.G., and Beutler, B. (2010). Slc15a4, AP-3, and Hermansky-Pudlak syndrome proteins are

required for Toll-like receptor signaling in plasmacytoid dendritic cells. Proceedings of the National Academy of Sciences of the United States of America *107*, 19973-19978.
Bosteels, C., Neyt, K., Vanheerswynghels, M., van Helden, M.J., Sichien, D., Debeuf, N., De Prijck, S., Bosteels, V., Vandamme, N., Martens, L.*, et al.* (2020). Inflammatory Type 2 cDCs Acquire Features of cDC1s and Macrophages to Orchestrate Immunity to Respiratory Virus Infection. Immunity *52*, 1039-1056 e1039.
Bryant, C., Fromm, P.D., Kupresanin, F., Clark, G., Lee, K., Clarke, C., Silveira, P.A., Suen, H., Brown, R., Newman, E.*, et al.* (2016). A CD2 high-expressing stress-resistant human plasmacytoid dendritic-cell subset. Immunol Cell Biol *94*, 447-457.
Cervantes-Barragan, L., Zust, R., Weber, F., Spiegel, M., Lang, K.S., Akira, S., Thiel, V., and Ludewig, B. (2007). Control of coronavirus infection through plasmacytoid dendritic-cell-derived type I interferon. Blood *109*, 1131-1137.
Chan, J.F., Kok, K.H., Zhu, Z., Chu, H., To, K.K., Yuan, S., and Yuen, K.Y. (2020). Genomic characterization of the 2019 novel human-pathogenic coronavirus isolated from a patient with atypical pneumonia after visiting Wuhan. Emerg Microbes Infect *9*, 221-236.
Channappanavar, R., Fehr, A.R., Vijay, R., Mack, M., Zhao, J., Meyerholz, D.K., and Perlman, S. (2016). Dysregulated Type I Interferon and Inflammatory Monocyte-Macrophage Responses Cause Lethal Pneumonia in SARS-CoV-Infected Mice. Cell host & microbe *19*, 181-193.
Chen, D.Y., Khan, N., Close, B.J., Goel, R.K., Blum, B., Tavares, A.H., Kenney, D., Conway, H.L., Ewoldt, J.K., Chitalia, V.C.*, et al.* (2021). SARS-CoV-2 disrupts proximal elements in the JAK-STAT pathway. Journal of virology, JVI0086221.
Chen, J., Lau, Y.F., Lamirande, E.W., Paddock, C.D., Bartlett, J.H., Zaki, S.R., and Subbarao, K. (2010). Cellular immune responses to severe acute respiratory syndrome coronavirus (SARS-CoV) infection in senescent BALB/c mice: CD4+ T cells are important in control of SARS-CoV infection. Journal of virology *84*, 1289-1301.
Colisson, R., Barblu, L., Gras, C., Raynaud, F., Hadj-Slimane, R., Pique, C., Hermine, O., Lepelletier, Y., and Herbeuval, J.P. (2010). Free HTLV-1 induces TLR7-dependent innate immune response and TRAIL relocalization in killer plasmacytoid dendritic cells. Blood *115*, 2177-2185.
Collart, M.A., Baeuerle, P., and Vassalli, P. (1990). Regulation of tumor necrosis factor alpha transcription in macrophages: involvement of four kappa B-like motifs and of constitutive and inducible forms of NF-kappa B. Mol Cell Biol *10*, 1498-1506.
Combes, A., Camosseto, V., N'Guessan, P., Arguello, R.J., Mussard, J., Caux, C., Bendriss-Vermare, N., Pierre, P., and Gatti, E. (2017). BAD-LAMP controls TLR9 trafficking and signalling in human plasmacytoid dendritic cells. Nat Commun *8*, 913.
Crouse, J., Kalinke, U., and Oxenius, A. (2015). Regulation of antiviral T cell responses by type I interferons. Nat Rev Immunol *15*, 231-242.
de Chassey, B., Aublin-Gex, A., Ruggieri, A., Meyniel-Schicklin, L., Pradezynski, F., Davoust, N., Chantier, T., Tafforeau, L., Mangeot, P.E., Ciancia, C.*, et al.* (2013). The interactomes of influenza virus NS1 and NS2 proteins identify new host factors and provide insights for ADAR1 playing a supportive role in virus replication. PLoS Pathog *9*, e1003440.
Decembre, E., Assil, S., Hillaire, M.L., Dejnirattisai, W., Mongkolsapaya, J., Screaton, G.R., Davidson, A.D., and Dreux, M. (2014). Sensing of immature particles produced by dengue virus infected cells induces an antiviral response by plasmacytoid dendritic cells. PLoS Pathog *10*, e1004434.

DeMali, K.A., Barlow, C.A., and Burridge, K. (2002). Recruitment of the Arp2/3 complex to vinculin: coupling membrane protrusion to matrix adhesion. The Journal of cell biology *159*, 881-891.
DeMali, K.A., Sun, X., and Bui, G.A. (2014). Force transmission at cell-cell and cell-matrix adhesions. Biochemistry *53*, 7706-7717.
Dreux, M., Garaigorta, U., Boyd, B., Decembre, E., Chung, J., Whitten-Bauer, C., Wieland, S., and Chisari, F.V. (2012). Short-range exosomal transfer of viral RNA from infected cells to plasmacytoid dendritic cells triggers innate immunity. Cell host & microbe *12*, 558-570.
Esashi, E., Bao, M., Wang, Y.H., Cao, W., and Liu, Y.J. (2012). PACSIN1 regulates the TLR7/9-mediated type I interferon response in plasmacytoid dendritic cells. Eur J Immunol *42*, 573-579.
Feng, E., Balint, E., Poznanski, S.M., Ashkar, A.A., and Loeb, M. (2021). Aging and Interferons: Impacts on Inflammation and Viral Disease Outcomes. Cells *10*.
Fong, T.C., Wu, Y., and Kipps, T.J. (1996). Identification of a promoter element that regulates tissue-specific expression of the human CD80 (B7.1) gene. J Immunol *157*, 4442-4450.
Galani, I.E., Rovina, N., Lampropoulou, V., Triantafyllia, V., Manioudaki, M., Pavlos, E., Koukaki, E., Fragkou, P.C., Panou, V., Rapti, V.*, et al.* (2021). Untuned antiviral immunity in COVID-19 revealed by temporal type I/III interferon patterns and flu comparison. Nature immunology *22*, 32-40.
Gandini, M., Gras, C., Azeredo, E.L., Pinto, L.M., Smith, N., Despres, P., da Cunha, R.V., de Souza, L.J., Kubelka, C.F., and Herbeuval, J.P. (2013). Dengue virus activates membrane TRAIL relocalization and IFN-alpha production by human plasmacytoid dendritic cells in vitro and in vivo. PLoS Negl Trop Dis *7*, e2257.
Gerardin, J.A., Baise, E.A., Pire, G.A., Leroy, M.P., and Desmecht, D.J. (2004). Genomic structure, organisation, and promoter analysis of the bovine (Bos taurus) Mx1 gene. Gene *326*, 67-75.
Gomez, J., Borras, F.E., Singh, R., Rajananthanan, P., English, N., Knight, S.C., and Navarrete, C.V. (2004). Differential up-regulation of HLA-DM, invariant chain, and CD83 on myeloid and plasmacytoid dendritic cells from peripheral blood. Tissue Antigens *63*, 149-157.
Grajales-Reyes, G.E., and Colonna, M. (2020). Interferon responses in viral pneumonias. Science (New York, N.Y *369*, 626-627.
Grant, C.E., Bailey, T.L., and Noble, W.S. (2011). FIMO: scanning for occurrences of a given motif. Bioinformatics *27*, 1017-1018.
Hadjadj, J., Yatim, N., Barnabei, L., Corneau, A., Boussier, J., Smith, N., Pere, H., Charbit, B., Bondet, V., Chenevier-Gobeaux, C.*, et al.* (2020). Impaired type I interferon activity and inflammatory responses in severe COVID-19 patients. Science (New York, N.Y *369*, 718-724.
Hiscott, J., Alper, D., Cohen, L., Leblanc, J.F., Sportza, L., Wong, A., and Xanthoudakis, S. (1989). Induction of human interferon gene expression is associated with a nuclear factor that interacts with the NF-kappa B site of the human immunodeficiency virus enhancer. Journal of virology *63*, 2557-2566.
Jing, Y., Shaheen, E., Drake, R.R., Chen, N., Gravenstein, S., and Deng, Y. (2009). Aging is associated with a numerical and functional decline in plasmacytoid dendritic cells, whereas myeloid dendritic cells are relatively unaltered in human peripheral blood. Hum Immunol *70*, 777-784.
Jolliffe, I.T., and Cadima, J. (2016). Principal component analysis: a review and recent developments. Philos Trans A Math Phys Eng Sci *374*, 20150202.

Kim, Y.M., and Shin, E.C. (2021). Type I and III interferon responses in SARS-CoV-2 infection. Exp Mol Med *53*, 750-760.
Kimura, I., Konno, Y., Uriu, K., Hopfensperger, K., Sauter, D., Nakagawa, S., and Sato, K. (2021). Sarbecovirus ORF6 proteins hamper induction of interferon signaling. Cell Rep *34*, 108916.
King, C., and Sprent, J. (2021). Dual Nature of Type I Interferons in SARS-CoV-2-Induced Inflammation. Trends Immunol *42*, 312-322.
Lauterbach, H., Bathke, B., Gilles, S., Traidl-Hoffmann, C., Luber, C.A., Fejer, G., Freudenberg, M.A., Davey, G.M., Vremec, D., Kallies, A.*, et al.* (2010). Mouse CD8alpha+ DCs and human BDCA3+ DCs are major producers of IFN-lambda in response to poly IC. The Journal of experimental medicine *207*, 2703-2717.
Lazear, H.M., Schoggins, J.W., and Diamond, M.S. (2019). Shared and Distinct Functions of Type I and Type III Interferons. Immunity *50*, 907-923.
Leal Rojas, I.M., Mok, W.H., Pearson, F.E., Minoda, Y., Kenna, T.J., Barnard, R.T., and Radford, K.J. (2017). Human Blood CD1c(+) Dendritic Cells Promote Th1 and Th17 Effector Function in Memory CD4(+) T Cells. Front Immunol *8*, 971.
Lee, S.K., Seo, S.H., Kim, B.S., Kim, C.D., Lee, J.H., Kang, J.S., Maeng, P.J., and Lim, J.S. (2005). IFN-gamma regulates the expression of B7-H1 in dermal fibroblast cells. J Dermatol Sci *40*, 95-103.
Lei, X., Dong, X., Ma, R., Wang, W., Xiao, X., Tian, Z., Wang, C., Wang, Y., Li, L., Ren, L.*, et al.* (2020). Activation and evasion of type I interferon responses by SARS-CoV-2. Nat Commun *11*, 3810.
Lenardo, M.J., Fan, C.M., Maniatis, T., and Baltimore, D. (1989). The involvement of NF-kappa B in beta-interferon gene regulation reveals its role as widely inducible mediator of signal transduction. Cell *57*, 287-294.
Li, Y., Renner, D.M., Comar, C.E., Whelan, J.N., Reyes, H.M., Cardenas-Diaz, F.L., Truitt, R., Tan, L.H., Dong, B., Alysandratos, K.D.*, et al.* (2021). SARS-CoV-2 induces double-stranded RNA-mediated innate immune responses in respiratory epithelial-derived cells and cardiomyocytes. Proceedings of the National Academy of Sciences of the United States of America *118*.
Li, Z., Ju, X., Silveira, P.A., Abadir, E., Hsu, W.H., Hart, D.N.J., and Clark, G.J. (2019). CD83: Activation Marker for Antigen Presenting Cells and Its Therapeutic Potential. Front Immunol *10*, 1312.
Libermann, T.A., and Baltimore, D. (1990). Activation of interleukin-6 gene expression through the NF-kappa B transcription factor. Mol Cell Biol *10*, 2327-2334.
Liu, T., Zhang, L., Joo, D., and Sun, S.C. (2017). NF-kappaB signaling in inflammation. Signal Transduct Target Ther *2*.
Lopez, J., Mommert, M., Mouton, W., Pizzorno, A., Brengel-Pesce, K., Mezidi, M., Villard, M., Lina, B., Richard, J.C., Fassier, J.B.*, et al.* (2021). Early nasal type I IFN immunity against SARS-CoV-2 is compromised in patients with autoantibodies against type I IFNs. The Journal of experimental medicine *218*.
Lucas, C., Wong, P., Klein, J., Castro, T.B.R., Silva, J., Sundaram, M., Ellingson, M.K., Mao, T., Oh, J.E., Israelow, B.*, et al.* (2020). Longitudinal analyses reveal immunological misfiring in severe COVID-19. Nature *584*, 463-469.
Macal, M., Jo, Y., Dallari, S., Chang, A.Y., Dai, J., Swaminathan, S., Wehrens, E.J., Fitzgerald-Bocarsly, P., and Zuniga, E.I. (2018). Self-Renewal and Toll-like Receptor Signaling Sustain

Exhausted Plasmacytoid Dendritic Cells during Chronic Viral Infection. Immunity *48*, 730-744 e735.
Makris, S., Paulsen, M., and Johansson, C. (2017). Type I Interferons as Regulators of Lung Inflammation. Front Immunol *8*, 259.
Mardia, K.V., Kent, J.T., and Bibby, J.M. (1979). Multivariate Analysis. Academic Press, London-New York-Toronto-Sydney-San Francisco *xv*, 502-502.
Marie, I., Durbin, J.E., and Levy, D.E. (1998). Differential viral induction of distinct interferon-alpha genes by positive feedback through interferon regulatory factor-7. The EMBO journal *17*, 6660-6669.
Matsuda, T., Almasan, A., Tomita, M., Uchihara, J.N., Masuda, M., Ohshiro, K., Takasu, N., Yagita, H., Ohta, T., and Mori, N. (2005). Resistance to Apo2 ligand (Apo2L)/tumor necrosis factor-related apoptosis-inducing ligand (TRAIL)-mediated apoptosis and constitutive expression of Apo2L/TRAIL in human T-cell leukemia virus type 1-infected T-cell lines. Journal of virology *79*, 1367-1378.
Matsui, T., Connolly, J.E., Michnevitz, M., Chaussabel, D., Yu, C.I., Glaser, C., Tindle, S., Pypaert, M., Freitas, H., Piqueras, B.*, et al.* (2009). CD2 distinguishes two subsets of human plasmacytoid dendritic cells with distinct phenotype and functions. J Immunol *182*, 6815-6823.
McGonagle, D., Sharif, K., O'Regan, A., and Bridgewood, C. (2020). The Role of Cytokines including Interleukin-6 in COVID-19 induced Pneumonia and Macrophage Activation Syndrome-Like Disease. Autoimmun Rev *19*, 102537.
McKinsey, T.A., Chu, Z., Tedder, T.F., and Ballard, D.W. (2000). Transcription factor NF-kappaB regulates inducible CD83 gene expression in activated T lymphocytes. Mol Immunol *37*, 783-788.
McLeay, R.C., and Bailey, T.L. (2010). Motif Enrichment Analysis: a unified framework and an evaluation on ChIP data. BMC Bioinformatics *11*, 165.
Merad, M., Sathe, P., Helft, J., Miller, J., and Mortha, A. (2013). The dendritic cell lineage: ontogeny and function of dendritic cells and their subsets in the steady state and the inflamed setting. Annu Rev Immunol *31*, 563-604.
Mesev, E.V., LeDesma, R.A., and Ploss, A. (2019). Decoding type I and III interferon signalling during viral infection. Nat Microbiol *4*, 914-924.
Mildner, A., and Jung, S. (2014). Development and function of dendritic cell subsets. Immunity *40*, 642-656.
Min, Y.Q., Huang, M., Sun, X., Deng, F., Wang, H., and Ning, Y.J. (2021). Immune evasion of SARS-CoV-2 from interferon antiviral system. Comput Struct Biotechnol J *19*, 4217-4225.
Miorin, L., Kehrer, T., Sanchez-Aparicio, M.T., Zhang, K., Cohen, P., Patel, R.S., Cupic, A., Makio, T., Mei, M., Moreno, E.*, et al.* (2020). SARS-CoV-2 Orf6 hijacks Nup98 to block STAT nuclear import and antagonize interferon signaling. Proceedings of the National Academy of Sciences of the United States of America *117*, 28344-28354.
Olayioye, M.A., Barisic, S., and Hausser, A. (2013). Multi-level control of actin dynamics by protein kinase D. Cell Signal *25*, 1739-1747.
Onodi, F., Bonnet-Madin, L., Meertens, L., Karpf, L., Poirot, J., Zhang, S.Y., Picard, C., Puel, A., Jouanguy, E., Zhang, Q.*, et al.* (2021). SARS-CoV-2 induces human plasmacytoid predendritic cell diversification via UNC93B and IRAK4. The Journal of experimental medicine *218*.
Park, A., and Iwasaki, A. (2020). Type I and Type III Interferons - Induction, Signaling, Evasion, and Application to Combat COVID-19. Cell host & microbe *27*, 870-878.

Pescarmona, R., Belot, A., Villard, M., Besson, L., Lopez, J., Mosnier, I., Mathieu, A.L., Lombard, C., Garnier, L., Frachette, C.*, et al.* (2019). Comparison of RT-qPCR and Nanostring in the measurement of blood interferon response for the diagnosis of type I interferonopathies. Cytokine *113*, 446-452.
Pizzorno, A., Padey, B., Julien, T., Trouillet-Assant, S., Traversier, A., Errazuriz-Cerda, E., Fouret, J., Dubois, J., Gaymard, A., Lescure, F.X.*, et al.* (2020). Characterization and Treatment of SARS-CoV-2 in Nasal and Bronchial Human Airway Epithelia. Cell Rep Med *1*, 100059.
Rebendenne, A., Valadao, A.L.C., Tauziet, M., Maarifi, G., Bonaventure, B., McKellar, J., Planes, R., Nisole, S., Arnaud-Arnould, M., Moncorge, O., and Goujon, C. (2021). SARS-CoV-2 triggers an MDA-5-dependent interferon response which is unable to control replication in lung epithelial cells. Journal of virology.
Reizis, B. (2019). Plasmacytoid Dendritic Cells: Development, Regulation, and Function. Immunity *50*, 37-50.
Rhodes, J.W., Tong, O., Harman, A.N., and Turville, S.G. (2019). Human Dendritic Cell Subsets, Ontogeny, and Impact on HIV Infection. Front Immunol *10*, 1088.
Rothlein, R., Dustin, M.L., Marlin, S.D., and Springer, T.A. (1986). A human intercellular adhesion molecule (ICAM-1) distinct from LFA-1. J Immunol *137*, 1270-1274.
Rotty, J.D., Wu, C., and Bear, J.E. (2013). New insights into the regulation and cellular functions of the ARP2/3 complex. Nat Rev Mol Cell Biol *14*, 7-12.
Sa Ribero, M., Jouvenet, N., Dreux, M., and Nisole, S. (2020). Interplay between SARS-CoV-2 and the type I interferon response. PLoS Pathog *16*, e1008737.
Saichi, M., Ladjemi, M.Z., Korniotis, S., Rousseau, C., Ait Hamou, Z., Massenet-Regad, L., Amblard, E., Noel, F., Marie, Y., Bouteiller, D.*, et al.* (2021). Single-cell RNA sequencing of blood antigen-presenting cells in severe COVID-19 reveals multi-process defects in antiviral immunity. Nat Cell Biol *23*, 538-551.
Saitoh, S.I., Abe, F., Kanno, A., Tanimura, N., Mori Saitoh, Y., Fukui, R., Shibata, T., Sato, K., Ichinohe, T., Hayashi, M.*, et al.* (2017). TLR7 mediated viral recognition results in focal type I interferon secretion by dendritic cells. Nat Commun *8*, 1592.
Sánchez, J. (1982). MARDIA, K. V., J. T. KENT, J. M. BIBBY: Multivariate Analysis. Academic Press, London-New York-Toronto-Sydney-San Francisco 1979. xv, 518 pp., $ 61.00. Biometrical Journal *24*, 502-502.
Sasai, M., Linehan, M.M., and Iwasaki, A. (2010). Bifurcation of Toll-like receptor 9 signaling by adaptor protein 3. Science (New York, N.Y *329*, 1530-1534.
Shakhov, A.N., Kuprash, D.V., Azizov, M.M., Jongeneel, C.V., and Nedospasov, S.A. (1990). Structural analysis of the rabbit TNF locus, containing the genes encoding TNF-beta (lymphotoxin) and TNF-alpha (tumor necrosis factor). Gene *95*, 215-221.
Shaw, J., Wang, Y.H., Ito, T., Arima, K., and Liu, Y.J. (2010). Plasmacytoid dendritic cells regulate B-cell growth and differentiation via CD70. Blood *115*, 3051-3057.
Shimizu, Y., van Seventer, G.A., Horgan, K.J., and Shaw, S. (1990). Costimulation of proliferative responses of resting CD4+ T cells by the interaction of VLA-4 and VLA-5 with fibronectin or VLA-6 with laminin. J Immunol *145*, 59-67.
Son, Y.H., Jeong, Y.T., Lee, K.A., Choi, K.H., Kim, S.M., Rhim, B.Y., and Kim, K. (2008). Roles of MAPK and NF-kappaB in interleukin-6 induction by lipopolysaccharide in vascular smooth muscle cells. J Cardiovasc Pharmacol *51*, 71-77.

Trouillet-Assant, S., Viel, S., Gaymard, A., Pons, S., Richard, J.C., Perret, M., Villard, M., Brengel-Pesce, K., Lina, B., Mezidi, M.*, et al.* (2020). Type I IFN immunoprofiling in COVID-19 patients. J Allergy Clin Immunol *146*, 206-208 e202.
Vanderbeke, L., Van Mol, P., Van Herck, Y., De Smet, F., Humblet-Baron, S., Martinod, K., Antoranz, A., Arijs, I., Boeckx, B., Bosisio, F.M.*, et al.* (2021). Monocyte-driven atypical cytokine storm and aberrant neutrophil activation as key mediators of COVID-19 disease severity. Nat Commun *12*, 4117.
Vanderheiden, A., Ralfs, P., Chirkova, T., Upadhyay, A.A., Zimmerman, M.G., Bedoya, S., Aoued, H., Tharp, G.M., Pellegrini, K.L., Manfredi, C.*, et al.* (2020). Type I and Type III Interferons Restrict SARS-CoV-2 Infection of Human Airway Epithelial Cultures. Journal of virology *94*.
Venables, W., and Ripley, B. (2002). Modern Applied Statistics with S Fourth edition.
Vicente-Manzanares, M., Choi, C.K., and Horwitz, A.R. (2009). Integrins in cell migration--the actin connection. Journal of cell science *122*, 199-206.
Villani, A.C., Satija, R., Reynolds, G., Sarkizova, S., Shekhar, K., Fletcher, J., Griesbeck, M., Butler, A., Zheng, S., Lazo, S.*, et al.* (2017). Single-cell RNA-seq reveals new types of human blood dendritic cells, monocytes, and progenitors. Science (New York, N.Y *356*.
Wang, W., Zhou, Z., Xiao, X., Tian, Z., Dong, X., Wang, C., Li, L., Ren, L., Lei, X., Xiang, Z., and Wang, J. (2021). SARS-CoV-2 nsp12 attenuates type I interferon production by inhibiting IRF3 nuclear translocation. Cell Mol Immunol *18*, 945-953.
Webster, B., Assil, S., and Dreux, M. (2016). Cell-Cell Sensing of Viral Infection by Plasmacytoid Dendritic Cells. Journal of virology *90*, 10050-10053.
Webster, B., Werneke, S.W., Zafirova, B., This, S., Coleon, S., Decembre, E., Paidassi, H., Bouvier, I., Joubert, P.E., Duffy, D.*, et al.* (2018). Plasmacytoid dendritic cells control dengue and Chikungunya virus infections via IRF7-regulated interferon responses. Elife *7*.
Wilson, D.H., Rissin, D.M., Kan, C.W., Fournier, D.R., Piech, T., Campbell, T.G., Meyer, R.E., Fishburn, M.W., Cabrera, C., Patel, P.P.*, et al.* (2016). The Simoa HD-1 Analyzer: A Novel Fully Automated Digital Immunoassay Analyzer with Single-Molecule Sensitivity and Multiplexing. J Lab Autom *21*, 533-547.
Wong, K.L., Tai, J.J., Wong, W.C., Han, H., Sem, X., Yeap, W.H., Kourilsky, P., and Wong, S.C. (2011). Gene expression profiling reveals the defining features of the classical, intermediate, and nonclassical human monocyte subsets. Blood *118*, e16-31.
Xia, H., Cao, Z., Xie, X., Zhang, X., Chen, J.Y., Wang, H., Menachery, V.D., Rajsbaum, R., and Shi, P.Y. (2020). Evasion of Type I Interferon by SARS-CoV-2. Cell Rep *33*, 108234.
Xie, X., Muruato, A., Lokugamage, K.G., Narayanan, K., Zhang, X., Zou, J., Liu, J., Schindewolf, C., Bopp, N.E., Aguilar, P.V.*, et al.* (2020). An Infectious cDNA Clone of SARS-CoV-2. Cell host & microbe.
Yamada, T., Sato, S., Sotoyama, Y., Orba, Y., Sawa, H., Yamauchi, H., Sasaki, M., and Takaoka, A. (2021). RIG-I triggers a signaling-abortive anti-SARS-CoV-2 defense in human lung cells. Nature immunology *22*, 820-828.
Yang, D., Chu, H., Hou, Y., Chai, Y., Shuai, H., Lee, A.C., Zhang, X., Wang, Y., Hu, B., Huang, X.*, et al.* (2020). Attenuated Interferon and Proinflammatory Response in SARS-CoV-2-Infected Human Dendritic Cells Is Associated With Viral Antagonism of STAT1 Phosphorylation. J Infect Dis *222*, 734-745.
Yao, C., Bora, S.A., Parimon, T., Zaman, T., Friedman, O.A., Palatinus, J.A., Surapaneni, N.S., Matusov, Y.P., Cerro Chiang, G., Kassar, A.G.*, et al.* (2021a). Cell-Type-Specific Immune Dysregulation in Severely Ill COVID-19 Patients. Cell Rep *34*, 108590.

Yao, C., Bora, S.A., Parimon, T., Zaman, T., Friedman, O.A., Palatinus, J.A., Surapaneni, N.S., Matusov, Y.P., Chiang, G.C., Kassar, A.G.*, et al.* (2021b). Cell-type-specific immune dysregulation in severely ill COVID-19 patients. Cell Rep *34*, 108943.
Yoshio, S., Kanto, T., Kuroda, S., Matsubara, T., Higashitani, K., Kakita, N., Ishida, H., Hiramatsu, N., Nagano, H., Sugiyama, M.*, et al.* (2013). Human blood dendritic cell antigen 3 (BDCA3)(+) dendritic cells are a potent producer of interferon-lambda in response to hepatitis C virus. Hepatology (Baltimore, Md *57*, 1705-1715.
Zhang, H., Gregorio, J.D., Iwahori, T., Zhang, X., Choi, O., Tolentino, L.L., Prestwood, T., Carmi, Y., and Engleman, E.G. (2017). A distinct subset of plasmacytoid dendritic cells induces activation and differentiation of B and T lymphocytes. Proceedings of the National Academy of Sciences of the United States of America *114*, 1988-1993.
Zhang, Q., Bastard, P., Liu, Z., Le Pen, J., Moncada-Velez, M., Chen, J., Ogishi, M., Sabli, I.K.D., Hodeib, S., Korol, C.*, et al.* (2020). Inborn errors of type I IFN immunity in patients with life-threatening COVID-19. Science (New York, N.Y *370*.
Zhao, J., Freeman, G.J., Gray, G.S., Nadler, L.M., and Glimcher, L.H. (1996). A cell type-specific enhancer in the human B7.1 gene regulated by NF-kappaB. The Journal of experimental medicine *183*, 777-789.
Zhou, Z., Ren, L., Zhang, L., Zhong, J., Xiao, Y., Jia, Z., Guo, L., Yang, J., Wang, C., Jiang, S.*, et al.* (2020). Heightened Innate Immune Responses in the Respiratory Tract of COVID-19 Patients. Cell host & microbe *27*, 883-890 e882.

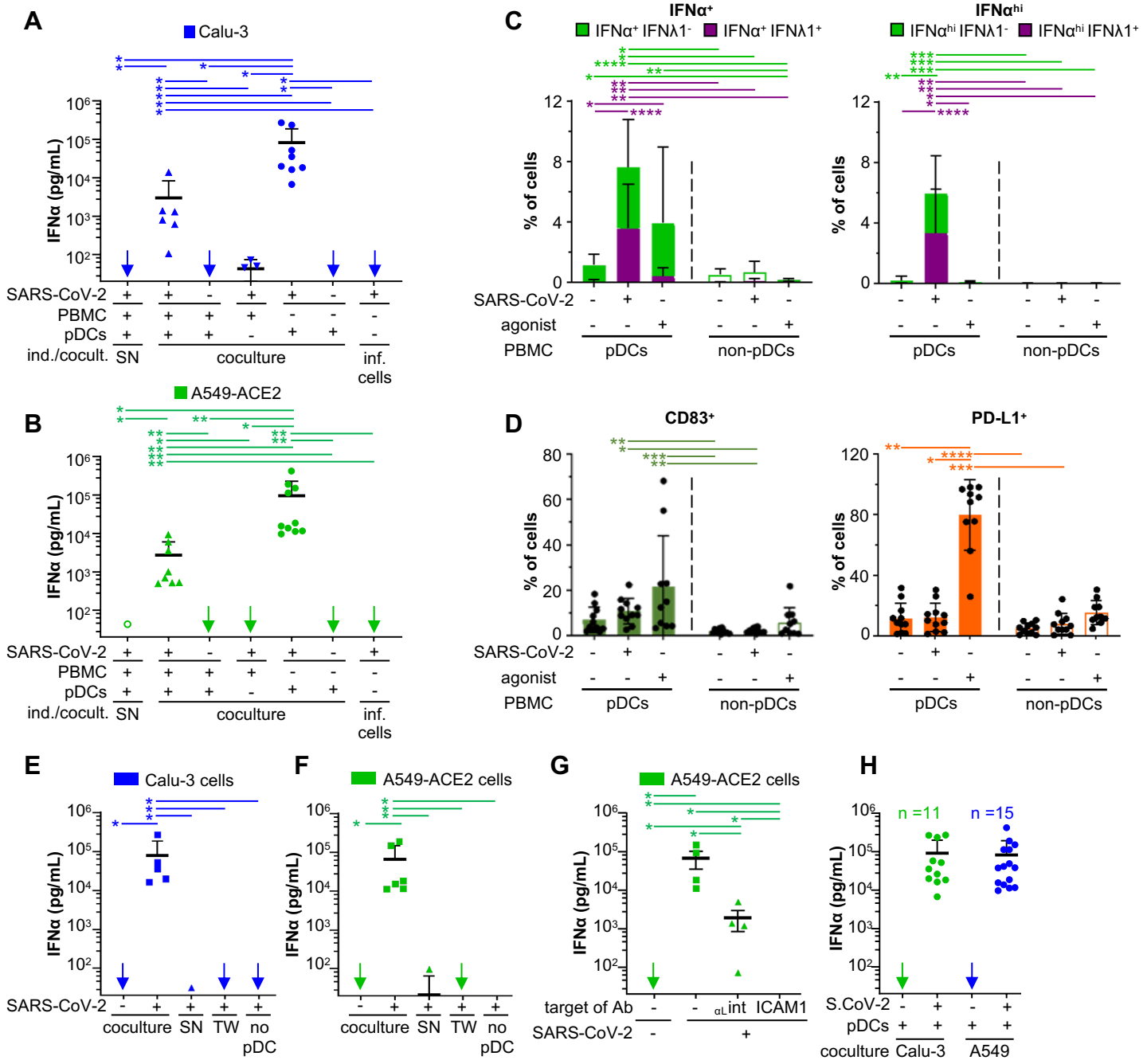
A
Calu-3
IFNα (pg/mL)
SARS-CoV-2
PBMC
pDCs
ind./cocult.
SN
coculture
inf. cells
B
A549-ACE2
C
IFNα+
IFNα+ IFNλ1-
IFNα+ IFNλ1+
IFNαhi
IFNαhi IFNλ1-
IFNαhi IFNλ1+
% of cells
agonist
pDCs
non-pDCs
D
CD83+
PD-L1+
E
Calu-3 cells
coculture
SN
TW
no pDC
F
A549-ACE2 cells
G
A549-ACE2 cells
target of Ab
αLint
ICAM1
H
n =11
n =15
S.CoV-2
coculture
Calu-3
A549

Figure 1

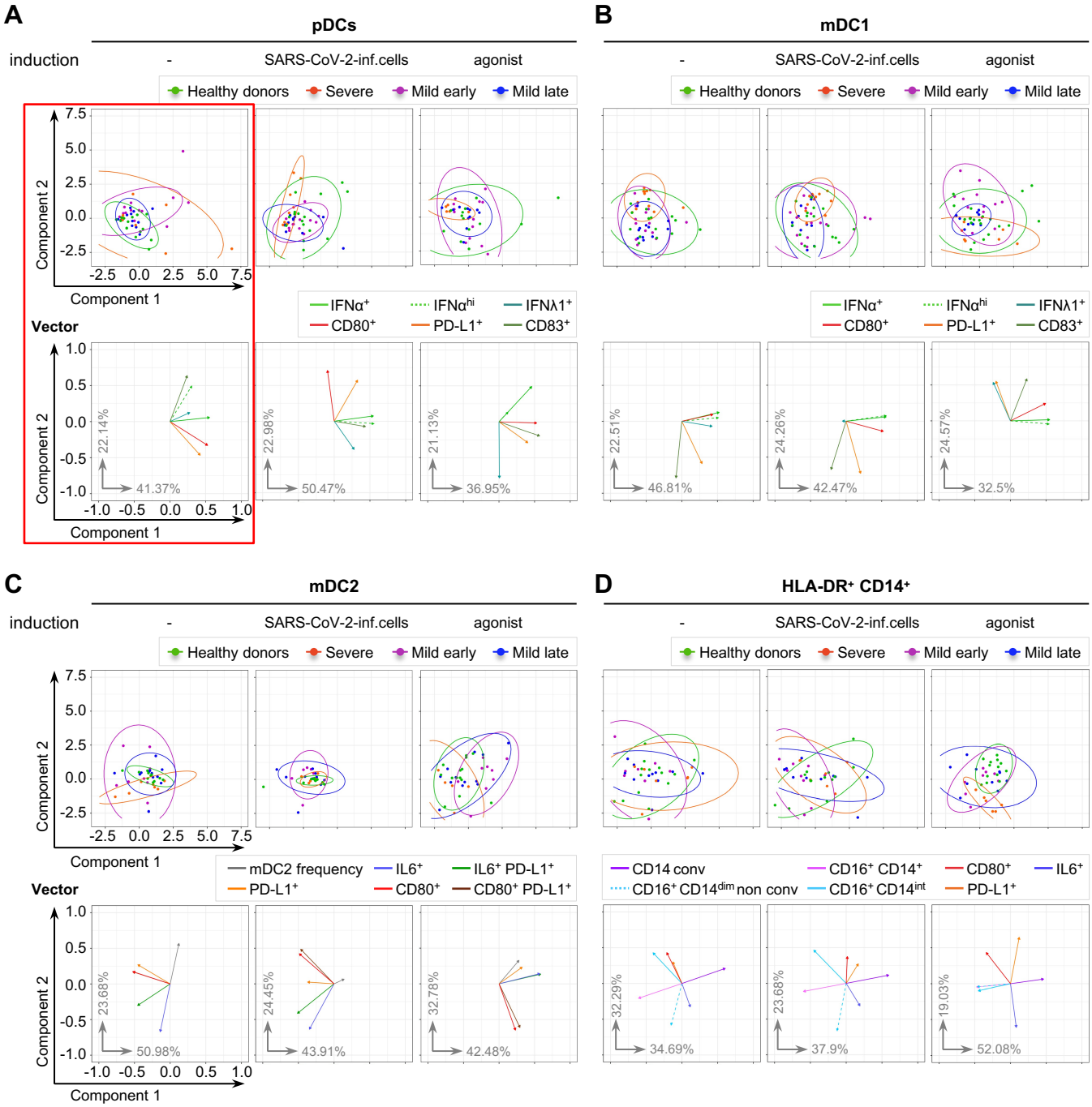
A
pDCs
induction
-
SARS-CoV-2-inf.cells
agonist
Healthy donors
Severe
Mild early
Mild late
Component 2
Component 1
Vector
IFNα+
IFNαhi
IFNλ1+
CD80+
PD-L1+
CD83+
22.14%
41.37%
22.98%
50.47%
21.13%
36.95%
B
mDC1
22.51%
46.81%
24.26%
42.47%
24.57%
32.5%
C
mDC2
mDC2 frequency
IL6+
IL6+ PD-L1+
PD-L1+
CD80+
CD80+ PD-L1+
23.68%
50.98%
24.45%
43.91%
32.78%
42.48%
D
HLA-DR+ CD14+
CD14 conv
CD16+ CD14+
CD80+
IL6+
CD16+ CD14dim non conv
CD16+ CD14int
PD-L1+
32.29%
34.69%
23.68%
37.9%
19.03%
52.08%

Figure 2

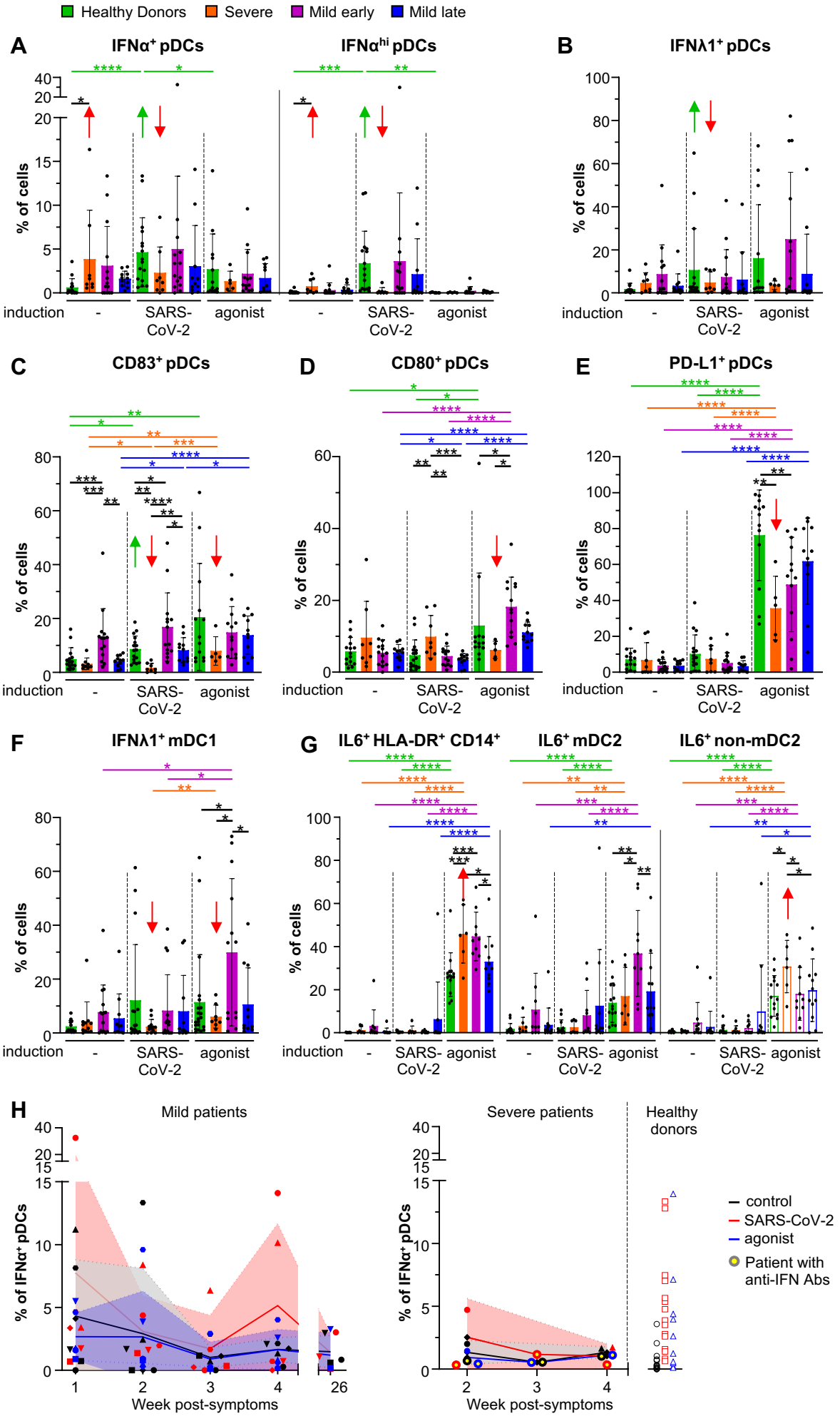
Healthy Donors
Severe
Mild early
Mild late
A
IFNα+ pDCs
IFNαhi pDCs
B
IFNλ1+ pDCs
C
CD83+ pDCs
D
CD80+ pDCs
E
PD-L1+ pDCs
F
IFNλ1+ mDC1
G
IL6+ HLA-DR+ CD14+
IL6+ mDC2
IL6+ non-mDC2
% of cells
induction
-
SARS-CoV-2
agonist
H
Mild patients
Severe patients
Healthy donors
% of IFNα+ pDCs
Week post-symptoms
control
SARS-CoV-2
agonist
Patient with anti-IFN Abs

Figure 3

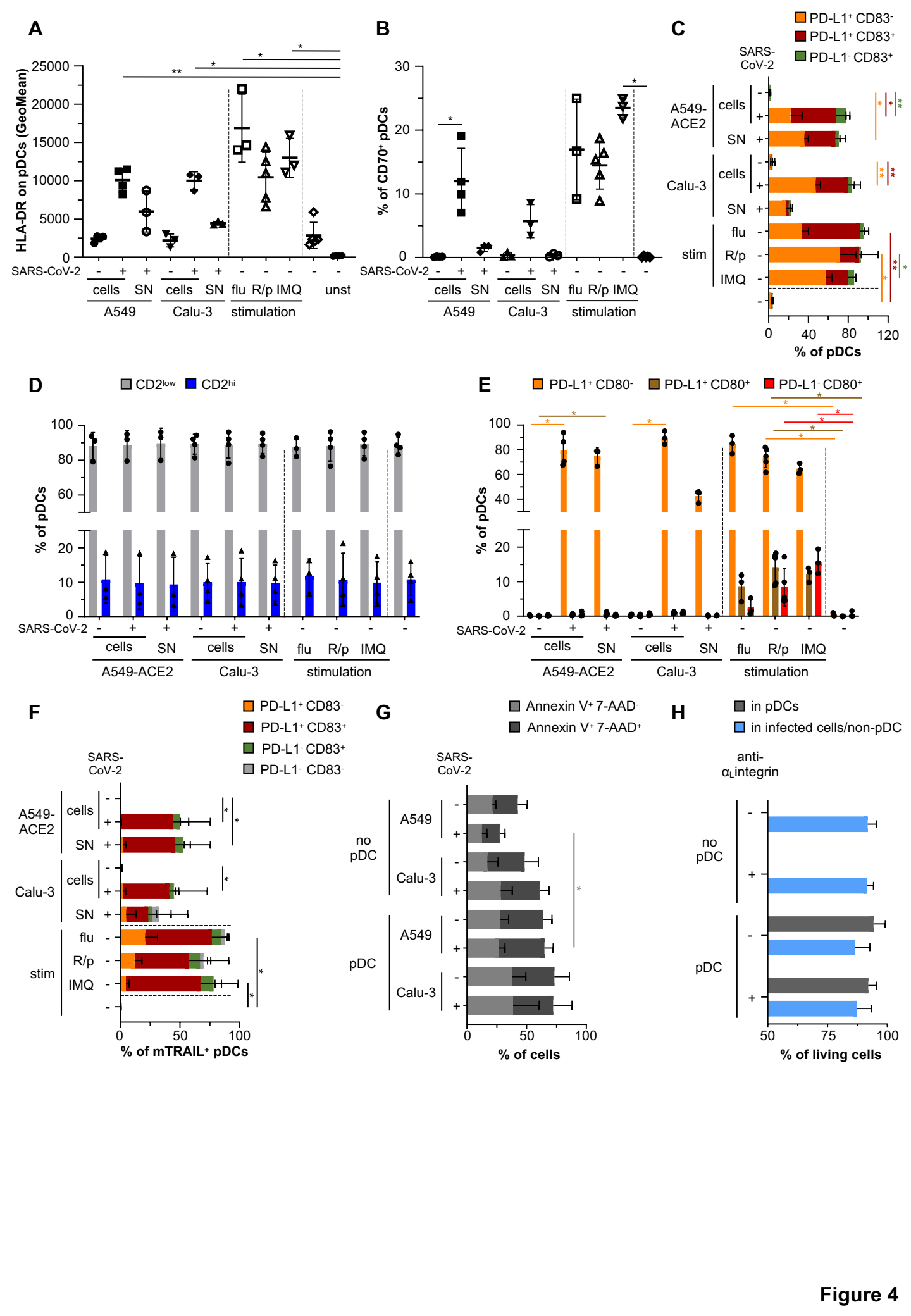
A
HLA-DR on pDCs (GeoMean)
SARS-CoV-2
cells SN cells SN flu R/p IMQ unst
A549 Calu-3 stimulation
B
% of CD70+ pDCs
C
PD-L1+ CD83-
PD-L1+ CD83+
PD-L1- CD83+
A549-ACE2
Calu-3
stim
% of pDCs
D
CD2low
CD2hi
A549-ACE2 Calu-3 stimulation
E
PD-L1+ CD80-
PD-L1+ CD80+
PD-L1- CD80+
F
PD-L1- CD83-
% of mTRAIL+ pDCs
G
Annexin V+ 7-AAD-
Annexin V+ 7-AAD+
no pDC
pDC
% of cells
H
in pDCs
in infected cells/non-pDC
anti-αLintegrin
% of living cells

Figure 4

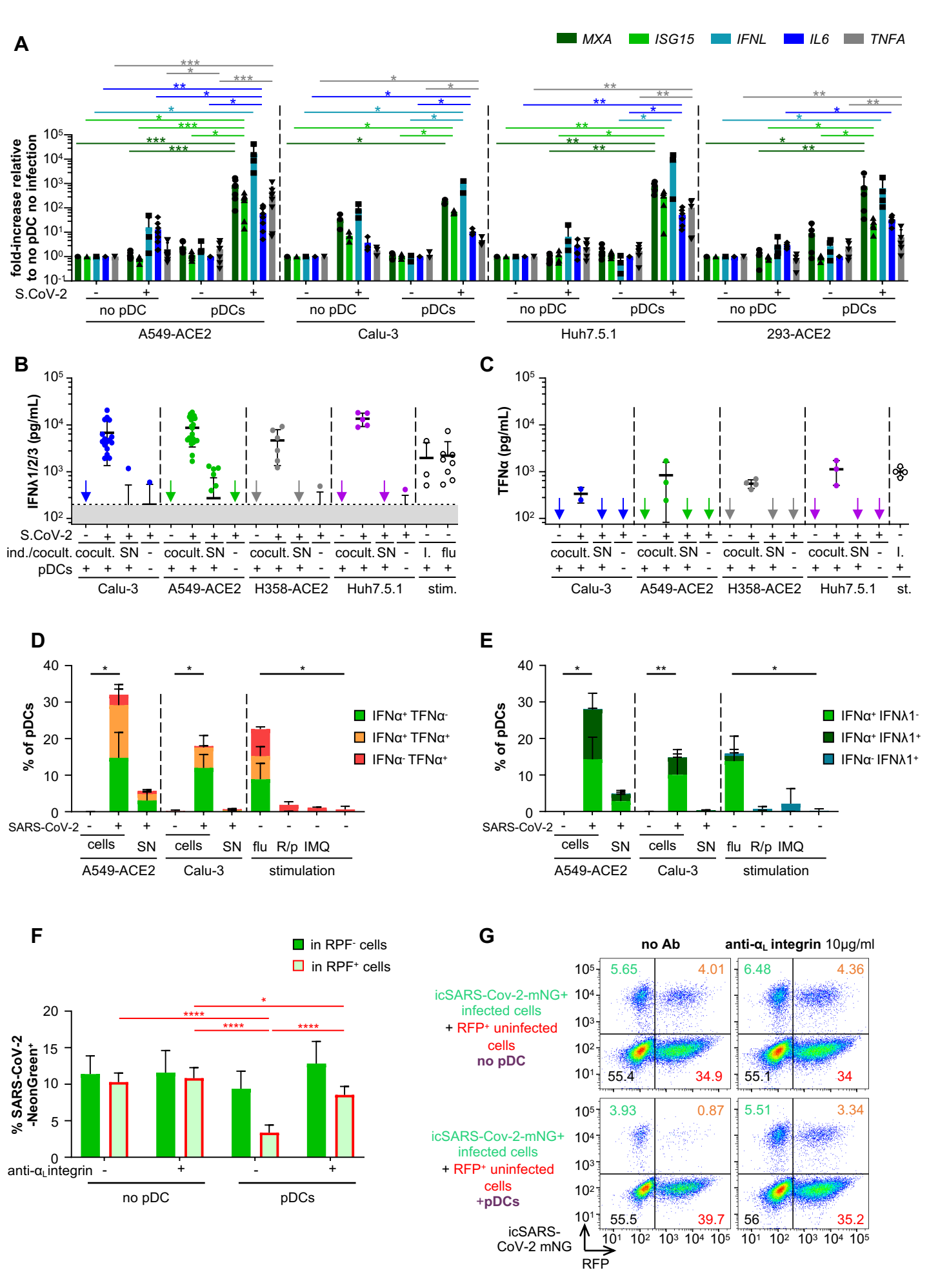
A
MXA
ISG15
IFNL
IL6
TNFA
fold-increase relative to no pDC no infection
S.CoV-2
no pDC
pDCs
A549-ACE2
Calu-3
Huh7.5.1
293-ACE2
B
IFNλ1/2/3 (pg/mL)
ind./cocult.
cocult.
SN
I.
flu
H358-ACE2
stim.
C
TFNα (pg/mL)
st.
D
% of pDCs
IFNα+ TFNα-
IFNα+ TFNα+
IFNα- TFNα+
SARS-CoV-2
cells
R/p
IMQ
stimulation
E
IFNα+ IFNλ1-
IFNα+ IFNλ1+
IFNα- IFNλ1+
F
in RPF- cells
in RPF+ cells
% SARS-CoV-2 -NeonGreen+
anti-αL integrin
G
no Ab
anti-αL integrin 10µg/ml
icSARS-Cov-2-mNG+ infected cells + RFP+ uninfected cells no pDC
icSARS-Cov-2-mNG+ infected cells + RFP+ uninfected cells +pDCs
icSARS-CoV-2 mNG
RFP

Figure 5

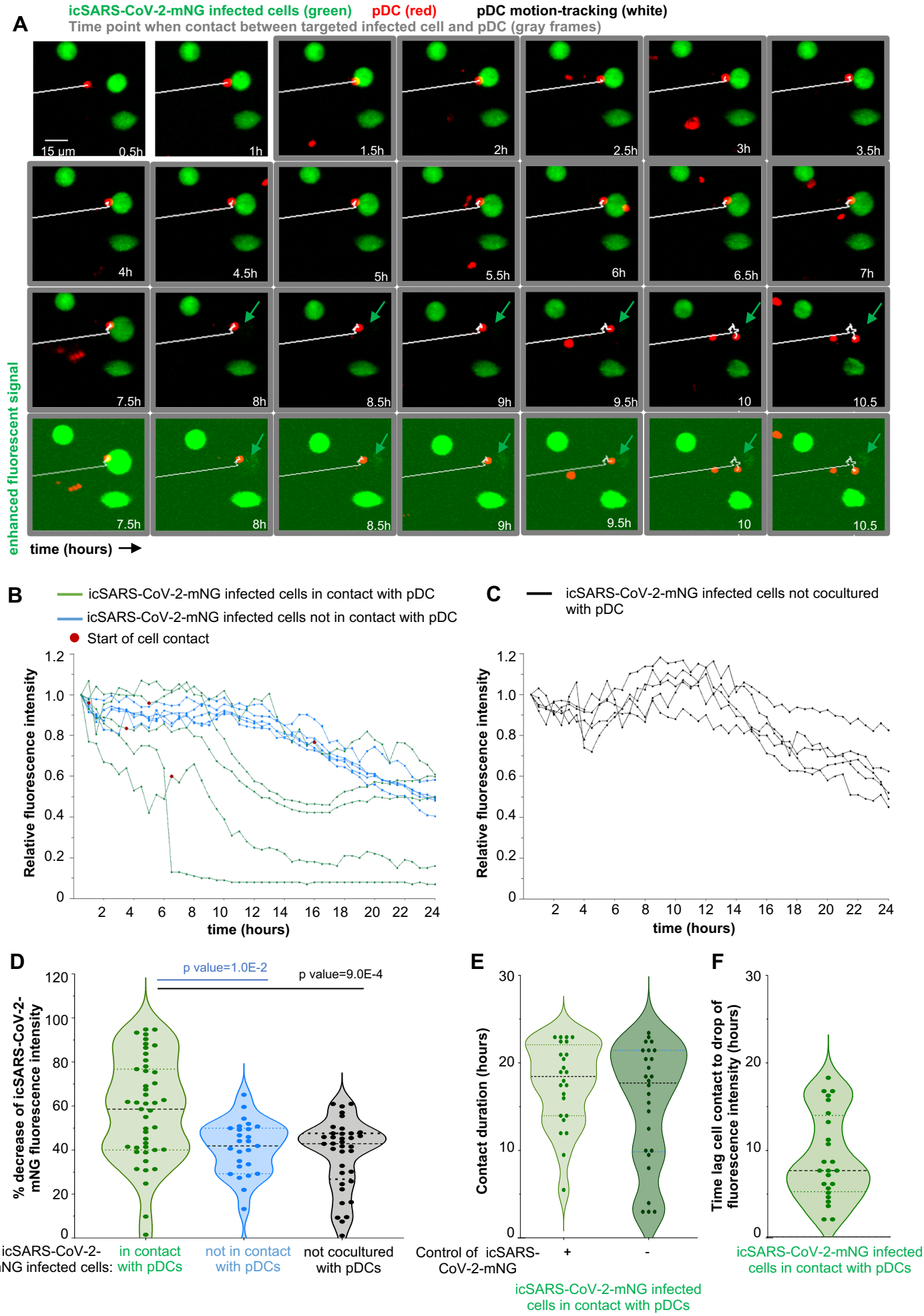
A
icSARS-CoV-2-mNG infected cells (green)
pDC (red)
pDC motion-tracking (white)
Time point when contact between targeted infected cell and pDC (gray frames)
15 µm
0.5h
1h
1.5h
2h
2.5h
3h
3.5h
4h
4.5h
5h
5.5h
6h
6.5h
7h
7.5h
8h
8.5h
9h
9.5h
10
10.5
enhanced fluorescent signal
time (hours)
B
icSARS-CoV-2-mNG infected cells in contact with pDC
icSARS-CoV-2-mNG infected cells not in contact with pDC
Start of cell contact
Relative fluorescence intensity
time (hours)
C
icSARS-CoV-2-mNG infected cells not cocultured with pDC
Relative fluorescence intensity
time (hours)
D
p value=1.0E-2
p value=9.0E-4
% decrease of icSARS-CoV-2-mNG fluorescence intensity
icSARS-CoV-2-mNG infected cells:
in contact with pDCs
not in contact with pDCs
not cocultured with pDCs
E
Contact duration (hours)
Control of icSARS-CoV-2-mNG
+
-
icSARS-CoV-2-mNG infected cells in contact with pDCs
F
Time lag cell contact to drop of fluorescence intensity (hours)
icSARS-CoV-2-mNG infected cells in contact with pDCs

Figure 6

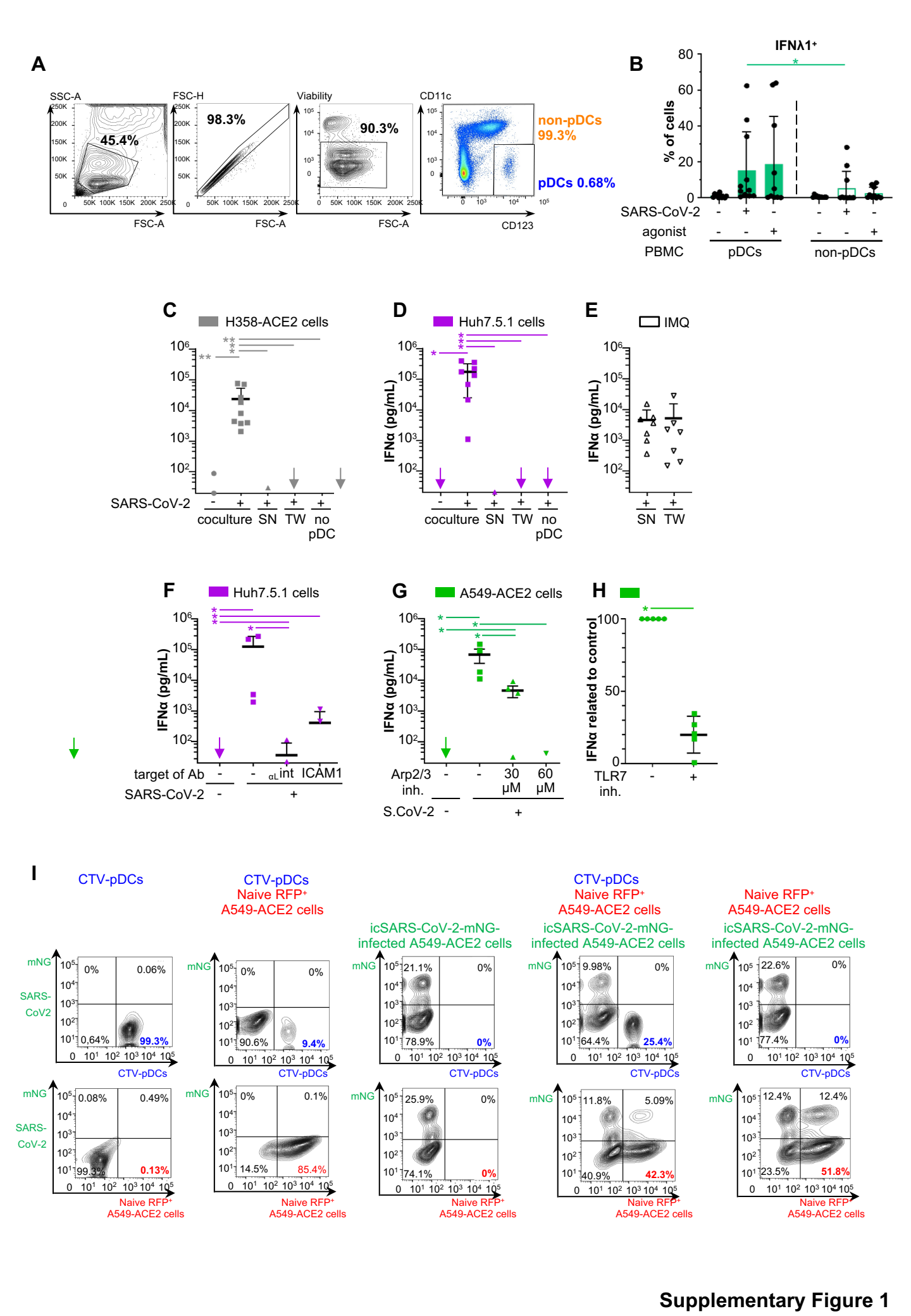

Supplementary Figure 1

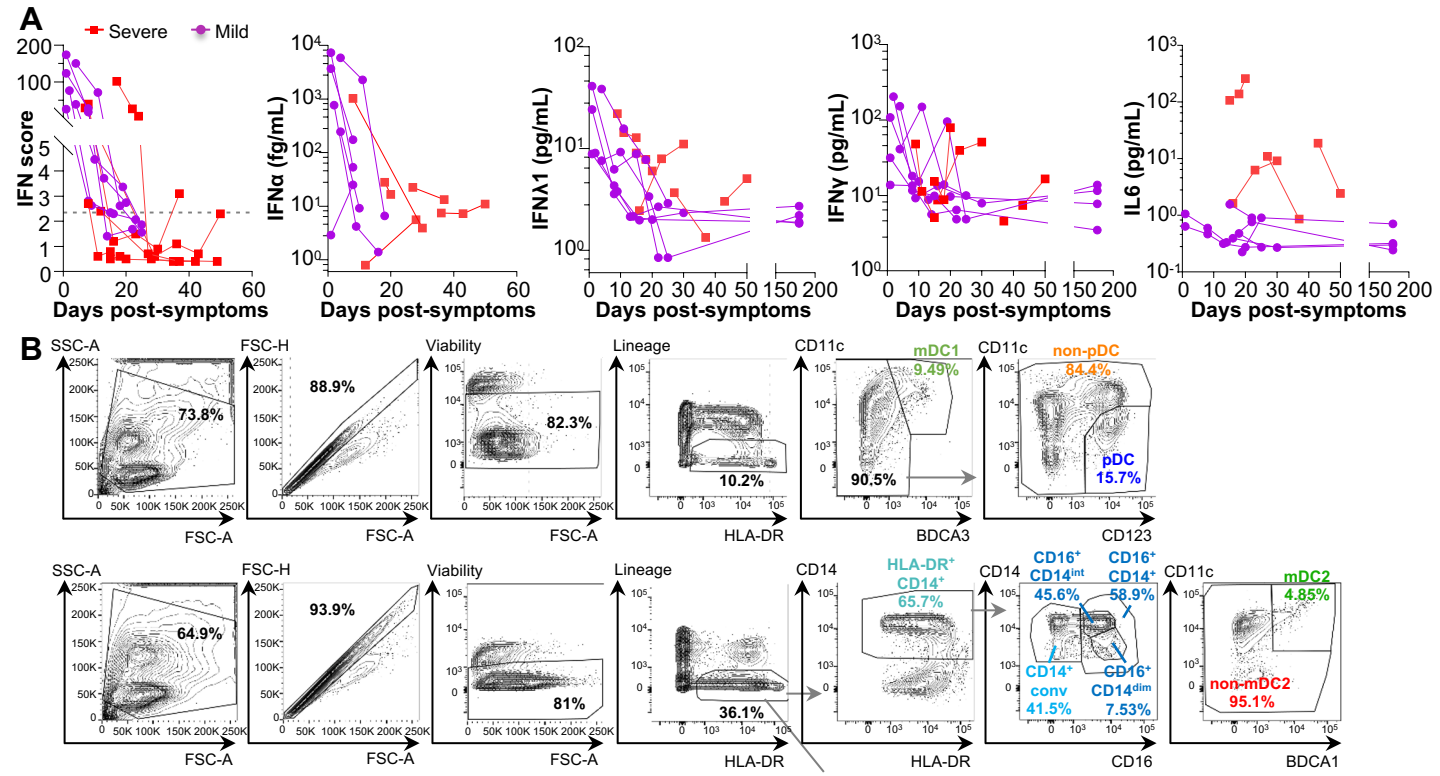

Supplementary Figure 2

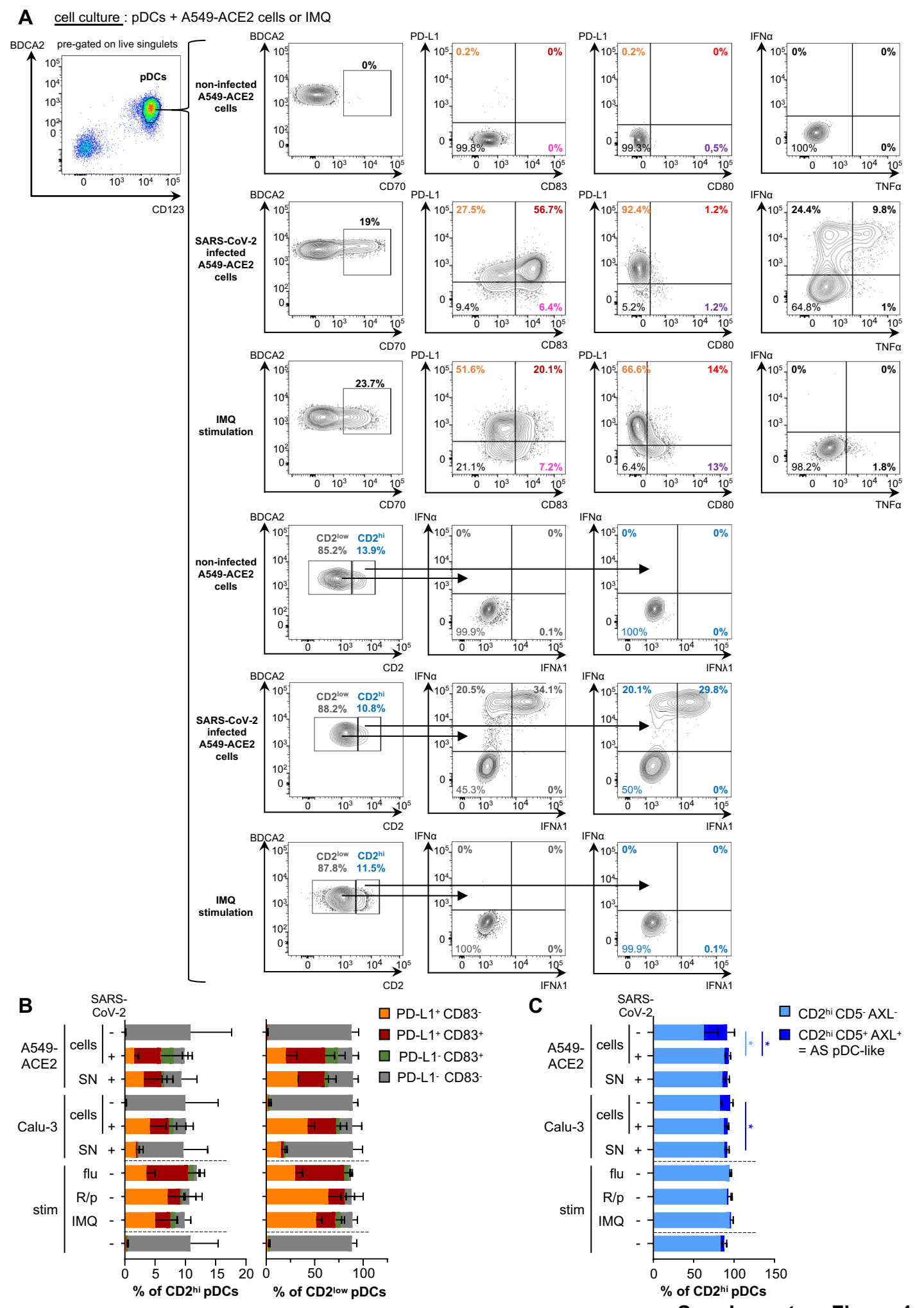

Supplementary Figure 4

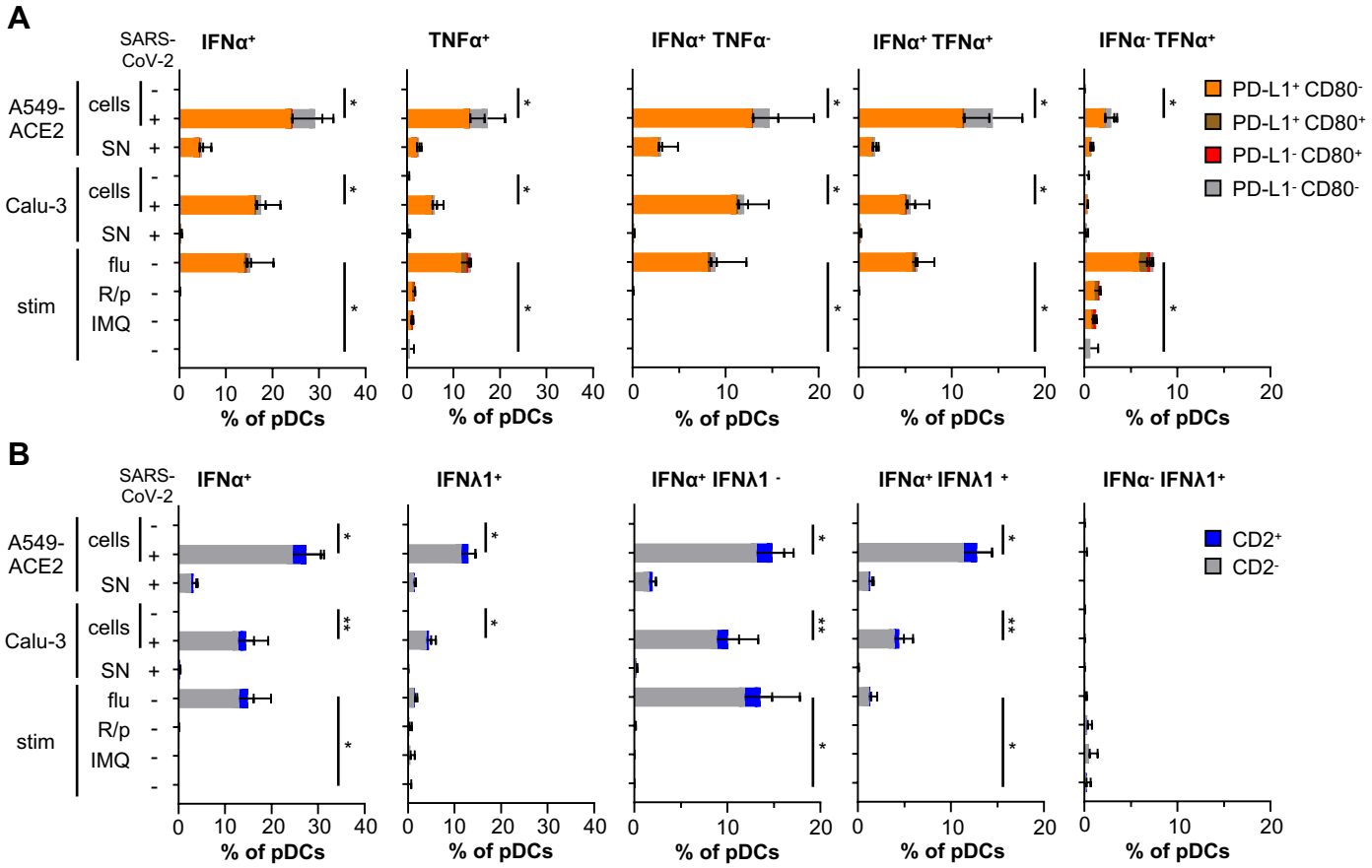

Supplementary Figure 5